Design of a Compact, Lightweight, and Low-Cost Solar Concentrator

by

Gabriel J. González

Submitted to the Department of Mechanical Engineering in Partial Fulfillment of the
Requirements for the Degree of

Bachelor of Science

at the

MASSACHUSETTS INSTITUTE OF TECHNOLOGY

February 2004

Signature of Author...
Department of Mechanical Engineering
February 06, 2004

Certified by..
Ernesto E. Blanco
Adjunct Professor of Mechanical Engineering
Thesis Supervisor

Accepted by..
Professor Ernest G. Cravalho
Chairman, Undergraduate Thesis Committee
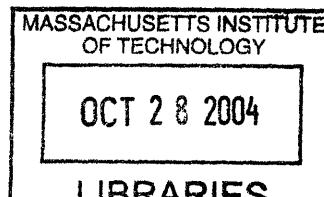
Design of a Compact, Lightweight, and Low-Cost Solar Concentrator

by

Gabriel J. González

Submitted to the Department of Mechanical Engineering
on February 6, 2004 in Partial Fulfillment of the Requirements for the
Degree of

Bachelor of Science

Abstract

The objective of this mechanical design project was to improve the current design of large and heavy solar concentrators. The three main design goals were: making the system compact, making the system lightweight, and minimizing expenses. The main approach to achieving these design parameters was to use the plastic film Mylar in its aluminized form to create a paraboloid serving as a solar concentrator. The scope of design was limited to designing and prototyping the solar concentrator, and neglecting to design and prototype the container in which it should be kept while in its compact form. Two designs—the tube design and the rim design—are examined, although the rim design is emphasized because of its advantages over the tube design. The tube design included a bicycle tire tube serving as the structural element of the solar concentrator, while the rim design utilized a bandsaw blade (without teeth) as the structural element of the solar concentrator. The prototype of the rim design proved to work well as a mirror, although further work, such as improving the seal around the rim, must still be done due to the time frame and resources allowed for this project.

Thesis Supervisor: Ernesto E. Blanco
Title: Adjunct Professor of Mechanical Engineering

Acknowledgements

This thesis project is very special to me because I not only learned about the design of solar concentrators, but I also learned a lot about myself and my capabilities. Completion of this thesis would not have been possible without the invaluable help and support provided to me by several people—People who I consider friends.

Professor Blanco, you have truly inspired me. Thank you for having confidence in me and teaching me much more than mechanical design. Thank you for teaching me much more than I have learned in any classroom or textbook at MIT, and also for your patience. You went the extra mile in being available when I needed your help. It is people like you who make MIT a much more enjoyable and memorable experience.

I would also like to thank everybody at the Pappalardo Lab, especially Steve Haberek. Steve, thanks for being so helpful with the welding during crunch time and for sharing your knowledge and humor. To the Pappalardo Lab staff, I admire you for your unmatched abilities in machining, your friendly personalities, and your ability to relate with the students you help so much everyday. Thanks for a 0% let-down rate in my four and a half years at MIT.

To Win Burleson, many thanks for being a genuinely nice guy and lending me a hand on short notice. Without your help deadlines would not have been met, and my thesis would not have been completed on time.

Two very special people in my life have provided me support 24 hours a day, seven days a week: Natalia Arzeno and Melissa González. Thank you for helping me out at all hours of the day, and for believing in me and keeping me motivated when I was discouraged. Thanks for being great friends.

Last, but not least, I would like to acknowledge my parents for all they have done for me. Mom and dad—Thanks for reminding me to turn to God when I was frustrated with life. Thank you for never neglecting any of my needs and making sacrifices for me so that I could have some opportunities that you were not blessed with growing up. I love you.

Table of Contents

List of Figures

1 Introduction

1.1 Motivation

Satellites have evolved immensely in a little over a third of a century. The launching of a satellite has gone from stopping in a nation's business activities to guaranteeing that they run like clockwork. Satellites have several applications, such as navigation, communications, environmental monitoring, and weather forecasting. Everyday life revolves around these services that satellites are making available to humans.

What is a satellite? A satellite is an object that orbits a larger object, such as a planet. Satellites are composed of three main parts:

- communication capabilities with Earth

- a power source

- a control system to accomplish its mission

If any of these three components of satellites were to fail, it would be catastrophic for the mission; therefore, the evolution of power sources for satellites is essential. The most convenient source of energy a satellite could take advantage of is solar energy.

Our planet depends on the Sun as its most important source of energy. Temperatures on the Sun's surface can reach up to about 6000 Kelvin. Nuclear fusion reactions occurring in the Sun's core allow it to produce approximately 386 billion billion megawatts of energy. Man has

created technologies that take advantage of solar energy and transforms it to other forms of energy, such as electric energy.

1.2 Background

The current problem with solar concentrators is that they are large and massive. Professor Ernesto Blanco, Adjunct Professor of the department of Mechanical Engineering at the Massachusetts Institute of Technology, suggested a design project for one of his classes, "Elements of Mechanical Design": a new design for solar concentrators for satellites. This design project aims to solve the problem of launching large and heavy solar concentrators along with satellites. Blanco's own description of the problem and solution are as follows:

Problem

One of the major problems associated with the use of solar energy is the cost of collectors. In the case of concentrator collectors the problem is even more serious. Besides that, variable focus solar concentrators do not exist. An attempt was made here to produce a concentrator of low cost and reasonably good optical characteristics.

Solution

For most applications where ideal optical characteristics are not essential, a rigid solid surface is hardly justifiable economically. In those cases reflecting films are more attractive. The only problem remaining is the cost of the frame. In the case of the concentrator mirror, the advantages of such a surface could justify the frame cost.

The concept of this film concentrator could not be simpler. A film of reflecting Mylar was attached to a steel dish of flat circular rim although not necessarily well made otherwise. The whole system was well sealed and in between was evacuated with a small vacuum pump. The surface of the taut Mylar film was depressed in a reasonably good optical shape. Only the boundaries showed imperfections. No focal temperatures were measured, but on a clear day wood would burn at the focus almost instantly. The focus could easily be varied by merely changing the pressure differential across the film surface. There may be some applications for this simple approach.

Professor Blanco's goal was to utilize aluminized Mylar to build solar concentrators of decreased weight and cost.

1.3   Scope of Design

The purpose of this mechanical design project was to design and prototype a solar concentrator for satellites that utilized Mylar as its reflective material. Specifically, this project focused on the design of a compactable solar concentrator, and neglected to design the solar concentrator's compacting container and its positioning system. Also, the solar collector attached to the end of the arm was a mockup made to represent where it would belong in the apparatus.

1.4   Design Goals

The three main design goals were:

- Make the system compactable

- Make the system lightweight

- Minimize expenses

Professor Blanco's idea of using Mylar as the mirror satisfies all three of these goals, but there are several ways in which one could utilize Mylar to make a solar concentrator.

The following describes two different approaches for designing and prototyping a solar concentrator: the tube design and the rim design. Emphasis is placed on the rim design, because that approach achieved better results.

2 Tube Design (Not Implemented)

The first design utilized a bicycle tire tube to create the circular structure of the solar concentrator. By intricately folding the deflated tube, the design goal of making the solar concentrator compact was easily achieved. Preliminary testing included folding the bicycle tire tube as shown in Figure 1. A rubber band was used to keep the folded tube in its folded position until the tube was inflated, triggering the rubber band to pop out, which allowed the tube to take its form; consequently, the solar concentrator unfolded and expanded, assuming the circular structure provided by the bicycle tire tube.

Figure 1: Photograph of the folding structure of the deflated bicycle tire tube structure

The large surface area surrounding the deflated bicycle tire tube in its folded state indicates the solar concentrator's ability of being very compact. Figure 2 makes it clear that the deflated bicycle tire tube accounts for less than 25% of the total solar concentrator surface area. This means that the solar concentrator could be reduced in size by over 75%.
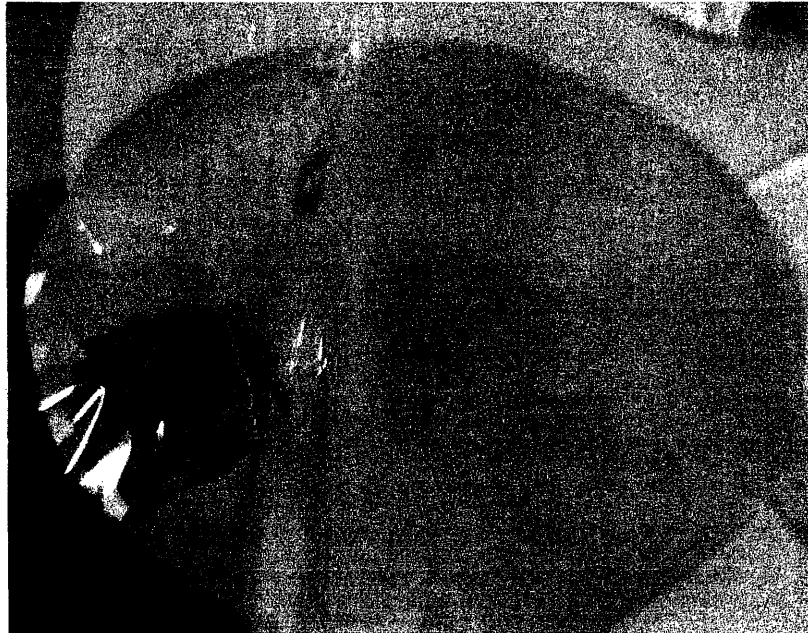
Figure 2: Photograph showing the small amount of space the folded bicycle tire tube occupies within the solar concentrator

The Presta valve attached to the bicycle tire tube was used to inflate the tube. In order to inflate the solar concentrator, a secondary air feed needed to be included. Keeping with Occam's razor—"Entities must not be multiplied beyond what is necessary"—the tube design was decided to include only one valve to feed air into the system for simplicity. To accomplish this goal, a small hole was punctured in the bicycle tire tube so that as the tube inflated, air would leak into the solar concentrator; consequently, the solar concentrator would also inflate, creating the parabolic shape of the reflecting Mylar film. Figure 3 explains how the dual inflation mechanism works. The hole punctured in the tube was deliberately made small so that the rate of air feed into the bicycle tire tube was greater than the rate of air feed into the solar concentrator. Theoretically, this would prevent air leaking into the solar concentrator at a premature state (i.e. before the bicycle tire tube was inflated enough to fully unfold the

concentrator and provide it structural support). The bicycle tire tube was expected to inflate completely, and at the same time the solar concentrator was expected to slowly inflate until they were both completely inflated and equilibrium was reached.
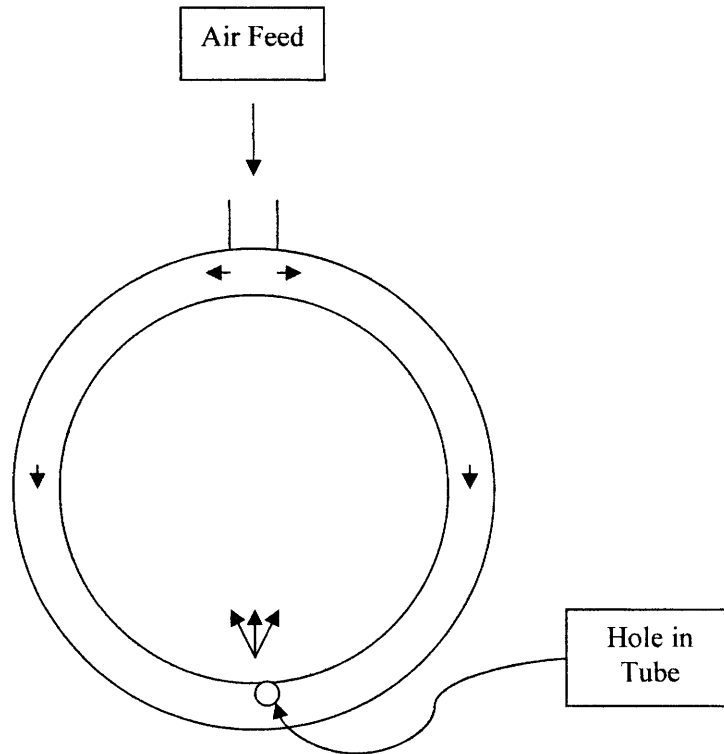
Figure 3: Diagram explaining the bicycle tire tube and solar concentrator dual inflation mechanism

Figure 4 shows the fully inflated solar concentrator. As can be seen, the optical quality of the Mylar reflecting film is poor. This was partially due to the bicycle tire tube not being rigid enough as a structural element inside the solar concentrator. As a result, the bicycle tire tube did not prevent radial stresses from reaching the area around the concentrator where the two sheets of Mylar were sealed together, causing a peeling effect. Due to the peeling effect, air could not

be pumped into the system to the point where the pressure inside the bicycle tire tube and the pressure inside the solar concentrator would reach equilibrium. The system was not pressurized enough, causing slack and poor optical characteristics.

Figure 4: Photograph of fully inflated tube design solar concentrator

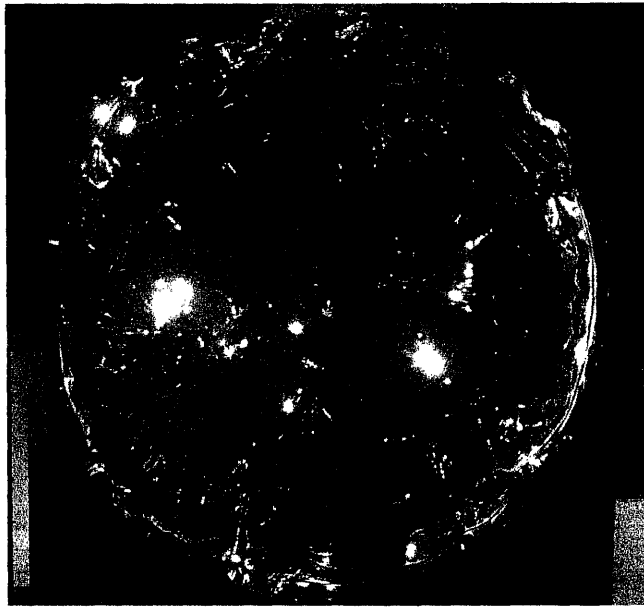Another drawback to the tube design is that the bicycle tire tube is not rigid enough to support an arm for the focal point. A strong, rigid structural element is required to sustain the moment that an arm would produce.

3 Rim Design (Implemented)

3.1 Design Overview

The rim design apparatus is shown in Figure 5. It includes two sheets of Mylar (one sheet of aluminized Mylar and one sheet of clear Mylar), a flexible rim, a support frame, a spring-loaded hinge, and an arm with the solar collector attached to it. The support frame is the base of the apparatus, on which the solar concentrator sits. The solar concentrator is clamped at both ends—one end is clamped by the spring-loaded hinge, and the other side is clamped with a C-clamp. The solar collector is positioned at the focal point of the paraboloid formed by inflating the solar concentrator. A Presta valve was inserted along the outer edge of the solar concentrator.
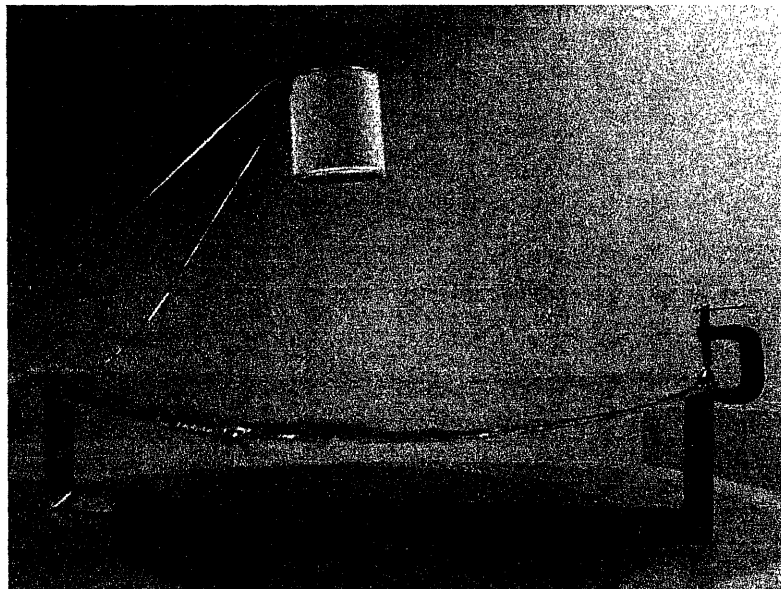
Figure 5: Photograph of solar concentrator apparatus

The solar concentrator is first folded in half, making it more compact. Then the concentrator is released and it springs open, allowing the arm and collector to also pop up into its position. Air is then pumped into the system through the Presta valve, and a paraboloid mirror/reflector is formed. This whole process can be seen in Figure 6.
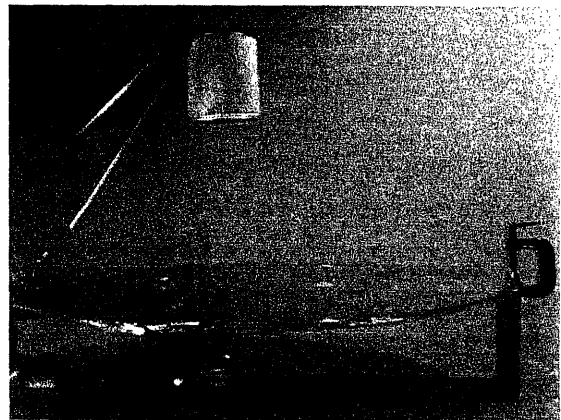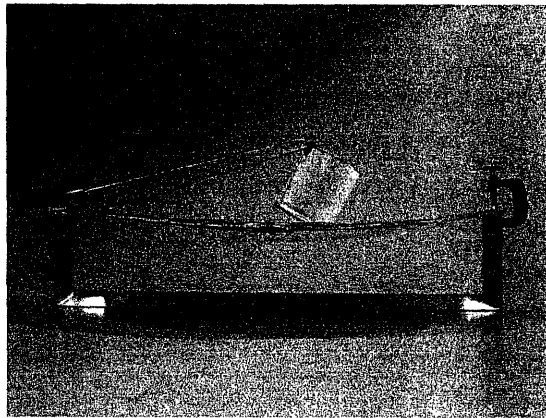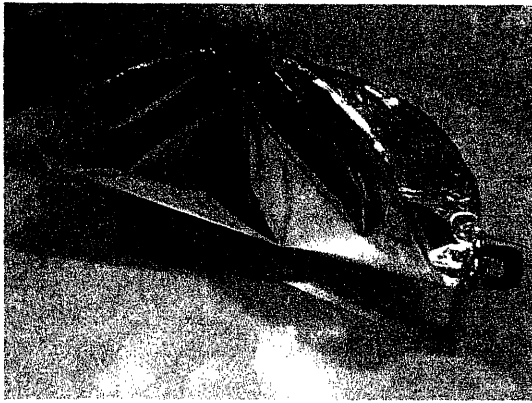
Figure 6: Photographs describing the process of the compacted solar concentrator opening up and being inflated.

The following sections will detail the mechanical components of the rim design.

3.1.1 Materials

Two different types of Mylar were used for the solar concentrator: clear Mylar (.001" thick) and aluminized Mylar (.002" thick). The Gund Company, Inc. describes Mylar as "...a flexible, strong and durable film with an unusual balance of properties making it suitable for many industrial applications. The excellent dielectric strength, moisture resistance and physical toughness make Mylar a very versatile and fully functioning insulating material."

Figure 7 includes some important material properties of Mylar.

Conductivity	0.0016 W/cm K
Specific Heat	1.883 J/g K
Density	1.309 g/cm^3
Melting Point	254 C

Figure 7: Table including some of Mylar's material properties—Conductivity, specific heat, density, and melting point

A bandsaw blade was used as the structural element inside the solar concentrator. Welding rod was shaped to make the arm holding the solar collector. The hinge and the support frame were both made out of aluminum.

3.1.2 Flexible Rim

The motivation for using a flexible rim sprouted from a Frisbee design. As Figure 8 shows, the compacted Frisbee on the palm of the hand (left picture) has a wire frame that is twisted a certain way so that it can fit into a small container. Once removed from the container, the Frisbee expands to the size shown in the right picture of Figure 8. The ratio of the expanded form of the frisbee to the compacted is 3:1.

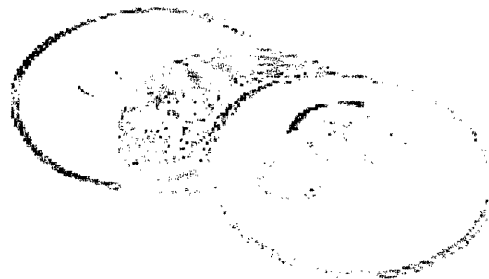Figure 8: Illustration of compactable Frisbee. Left picture shows the Frisbee in its compact form; Right picture shows the Frisbee in its expanded form.

A bandsaw blade was utilized as the rim of the solar concentrator system. As a rough cut, the teeth of the blade were cut off and the remaining material was grinded down using the belt sander to produce a rim 1/8" wide. Both edges of the rim were made smooth so that it would not

puncture the Mylar in any way, promoting an airtight seal. The two ends of the bandsaw blade were overlapped as shown in Figure 9. In order to conform to the design of a 20" diameter, the length of the overlap was 1.5". The overlap was then wrapped tightly with wire and expoxy was used to bind the two ends of the bandsaw blade together along with the wrapped wire. This proved to be an excellent joint. It could withstand a considerate amount of tension and shear, providing still some flexibility.
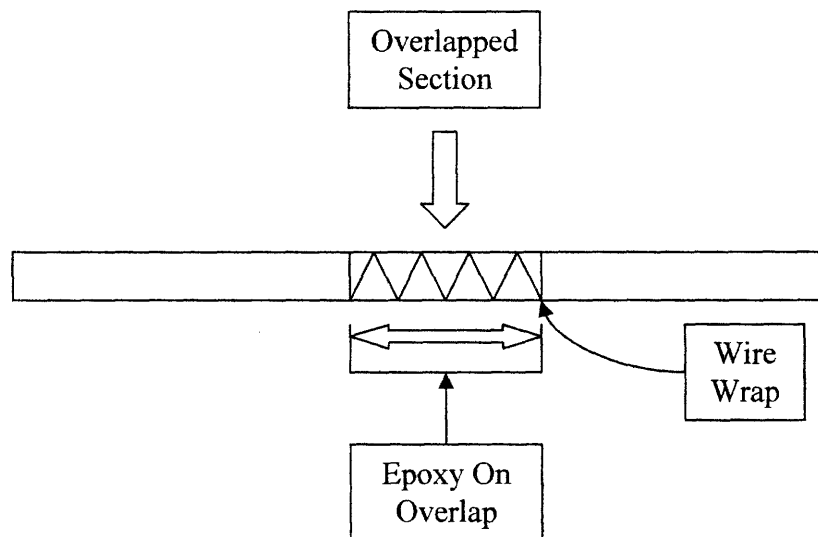
Figure 9: Top view diagram illustrating the joining of the two ends of the bandsaw blade used to form the rim for the solar concentrator

Twisting the rim in three dimensions, as the Frisbee approach requires, caused a couple of problems. The rim showed deformation in its expanded form. Also, twisting the rim in such a manner induced high stresses on the Mylar sheets, which put them in danger of tearing and scratching, causing air leakage and poor optical characteristics.

A compromise was made in the manner of twisting the solar concentrator system in order to prevent any catastrophic events such as tearing and scratching of the Mylar sheets. Bending the rim along one plane worked much better than the previous method of bending the rim along multiple planes (three-dimensional bending). Very little deformation was evident after the solar concentrator was expanded and the stress on the Mylar sheets was significantly lower. As a drawback, the solar concentrator was less compact. The ratio of the expanded form of the solar concentrator to the compact form of the concentrator was 2:1.

3.1.3 Sealing the System

Perhaps the most critical component of the solar concentrator system is the airtight seal it requires. Sealing the system was difficult for a myriad of reasons. For one, the resources available in the short period of time (one month) were few.

The first approach to sealing the system was to use a heat sealer. Local hardware stores did not carry them, so one was purchased from an online company. The purchased heat sealer can be seen in Figure 10. When first used, it was noted that only straight seals could be made, making it difficult to achieve the goal of creating the circular shape needed for a parabolic concentrator. Figure 11 shows the type of seal actually made by the heat sealer purchased. Not only did the sealer produce an undesired shape, it was also very time consuming. This idea was terminated, due to its insufficiency in achieving design goals.
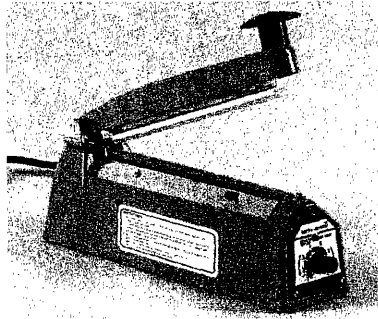
Figure 10: Photograph of sealer purchased online (only produces straight seals)
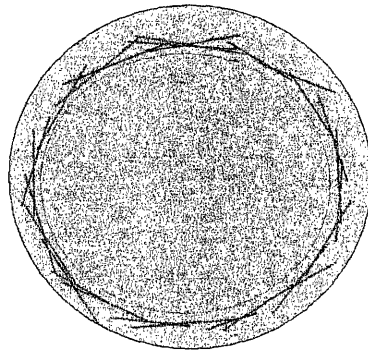
Figure 11: Imitation of system sealed by the straight heat sealer

A heat sealer with curved sealing capabilities was sought out. Several expensive heat sealers of this type were found online. The Eurosealer, whose primary function is to seal opened potato chip bags, was selected as the next approach to heat sealing the system. It was capable of making curved seals, and it was much less expensive than the other heat sealers. Minimizing expenses was extremely important, since the budget was tight.

The diagram on the left side in Figure 12 shows the layout of the materials used to facilitate the sealing with the Eurosealer. The aluminized Mylar was placed on the surface of a table. The rim

was then placed over the sheet of aluminized Mylar with the sheet of clear Mylar on top of it. A rim of slightly larger diameter was made (using the same process as the production of the solar concentrator rim). This rim was then placed around the solar concentrator rim, which served two main purposes—it held the two sheets of Mylar closely together, and it also served as a guide for the Eurosealer to follow a circular path.

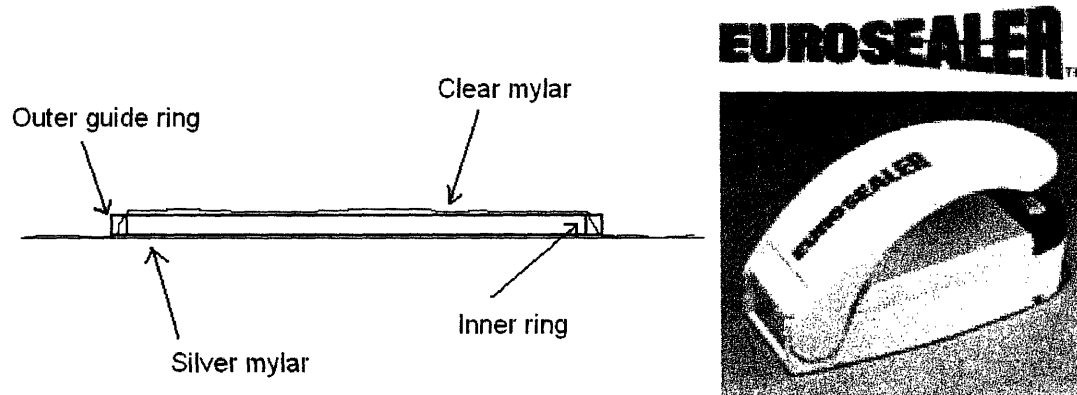Figure 12: Left, a diagram of the positioning of materials used to guide the Eurosealer in a circular path; Right, a photograph of the Eurosealer

The Eurosealer approach failed in that the seals were too weak, and again, it was time consuming to use.

Other instruments were tested for their heat sealing capabilities:

- soldering iron

- clothes iron

- hair-straightening iron

23

- flame from lighter

These approaches all failed to seal the solar concentrator system in a desirable way. The soldering iron and the lighter flame both melted the two sheets of Mylar together. The main problem with these two instruments was that they had little control in the way they sealed because they melted the plastics too quickly. On the other hand, the clothes iron and the hair-straightening iron had little sealing capability, if any at all.

Ultrasonic welding was the next approach taken. Ultrasonic Metal Welding, a book by STAPLA Ultrasonics Corporation, describes ultrasonic plastic welding:

> "Ultrasonic welding of plastics is a state-of-the-art technology that has been in use for many years. When welding thermoplastics, the thermal rise in the bonding area is produced by the absorption of mechanical vibrations, the reflection of the vibrations in the connecting area, and the friction of the surfaces of the parts. The vibrations are introduced vertically. In the contraction area, frictional heat is produced so that material plasticizes locally, forging an insoluble connection between both parts within a very short period of time.
>
> The prerequisite is that both working pieces have a near equivalent melting point. The joint quality is very uniform because the energy transfer and the released internal heat remains constant and is limited to the joining area. In order to obtain an optimum result, the joining areas are prepared to make them suitable for ultrasonic bonding. Besides plastics welding, ultrasonics can also be used to rivet working parts or embed metal parts into plastic."

Limited access was granted for use of the ultrasonic welding machine at the M.I.T. Media Laboratory for the available time frame; therefore, it was assumed that the ultrasonic welder would only be used one time. Figure 13 shows two different views of the same solar concentrator sealed using the ultrasonic welding machine. The ultrasonic welding machine

allowed for the option between two different types of seals. One type of seal was thin and it cut the excess Mylar material simultaneous to the sealing. The other type of seal was a double seal. The inner seal was a strong, thick seal and the outer seal was the same as the thin seal previously mentioned. The inner seal was not airtight, but acted as a reinforcement element, preventing the thin seal to peel.

Unfortunately, the time frame allowed for using the ultrasonic welding machine was too small to master the art of creating an excellent double seal for the solar concentrator. However, the single seal was used and the results were still better than any of the other previous approaches to sealing the system. The process of making the seal included placing the two sheets of Mylar together so that they are flat (without the rim), drawing a circle of 20" diameter (same as the rim) on one of the sheets, and welding the two sheets together along the drawn circle. A small 4" arc length was left unsealed, at which point we inserted the rim by bending it until it fit in the open area. The unsealed area was then sealed with the ultrasonic welding machine. As shown in Figure 13, the two Mylar sheets were welded together and fit tightly against the rim.
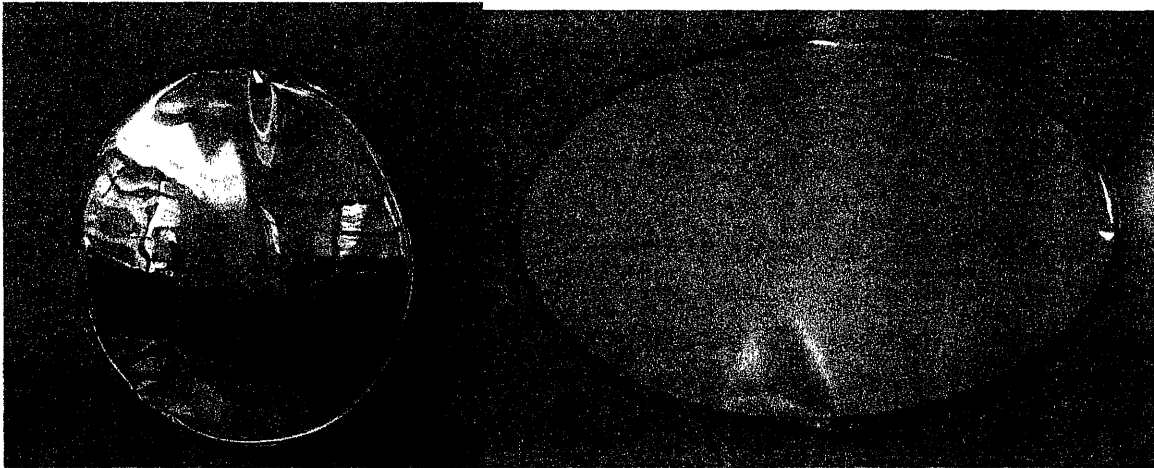
Figure 13: Photographs of two views of solar concentrator sealed using and ultrasonic welding machine

Epoxy was spread along the outer edge of the welded sheets of Mylar. This was done in order to cover up any small holes that may be present due to bad welding. Also, adding epoxy reinforced the weld. A Presta valve was attached to the outer edge of the solar concentrator by cutting out a small hole on the Mylar. The hole was just big enough to squeeze a third of the Presta valve inside the solar concentrator, and was placed at an angle to the rim, rather than perpendicular to it. The Presta valve was sealed to the Mylar sheets by adding Epoxy to fill in the gap. The seal was tested by inflating the solar concentrator by connecting the Presta valve to a bicycle pump fitting. Once fully inflated, the solar concentrator produced a decent mirror, as Figure 14 shows. The solar concentrator slowly deflated, indicating a flaw in the seal. The ultrasonic welding did show a great improvement over previous methods of sealing the system; not only did the interval between full inflation and full deflation increase, but the seal was able to withstand a higher pressure with little to no peeling effect.
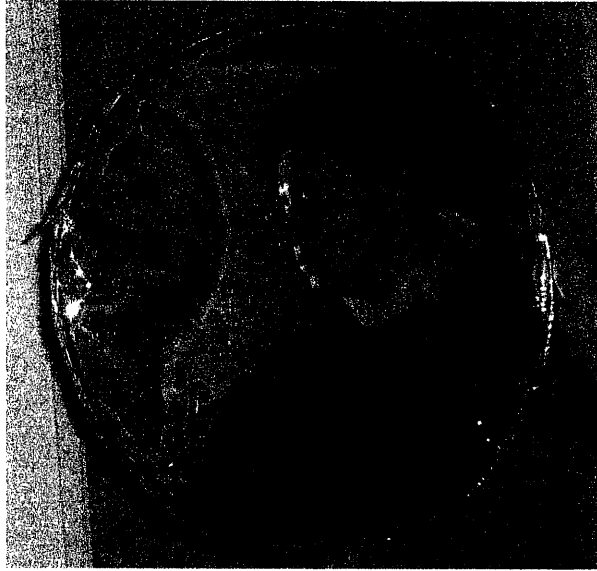
Figure 14: Photograph of inflated solar concentrator showing decent optical quality

The quality of the reflection in Figure 14 would have been even better had the aluminized Mylar been kept in better condition prior to the sealing.

3.1.4 Hinge

The hinge component (Figure 15) served both as a clamp for the solar concentrator rim, and as a pivot for the arm supporting the focus point (solar collector). It was made out of sheet aluminum 1/16" thick. The sheet aluminum was clamped and hammered into a 'U' shape, leaving a middle gap of about 1/8" width. Two holes were drilled using the drill press and 10-32 bolts were inserted. As the nuts and bolts were tightened, the two sides of the 'U' slowly closed together, causing a clamping effect on the portion of the solar concentrator rim that was inserted in the gap.
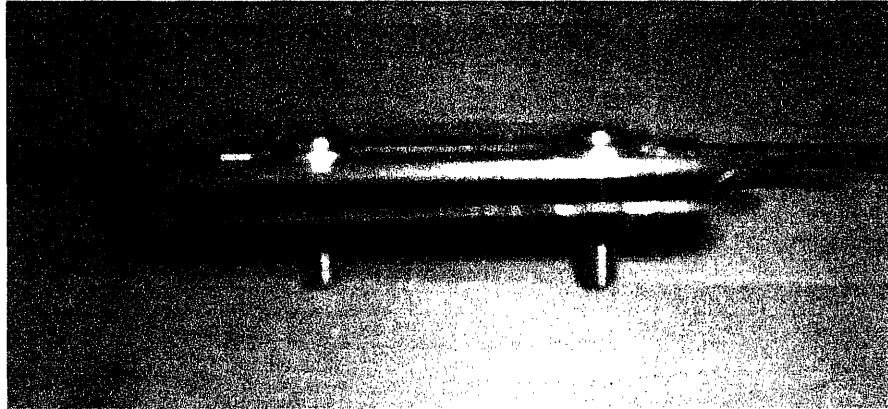
Figure 15: Photograph of the hinge component (front view)

The top view of the hinge component is shown in Figure 16. In this photograph, the pivot and spring mechanism is shown. A plastic tube of diameter slightly larger than that of the welding rod (used for the arm that supports the focus point) was cut and wrapped with wire to prevent it from cracking. Two small holes were drilled on the bottom part of the 'U'. One on each side of the plastic tube, and in each of the holes a leg of a torsion spring is inserted. The two torsion springs can be seen in Figure 16. These torsion springs offered a resistance when it was attempted to close the arm (pivot it so that the focus point gets closer to the solar concentrator). The tube was attached to the hinge component with epoxy. Welding rod was used as the material for the arm.
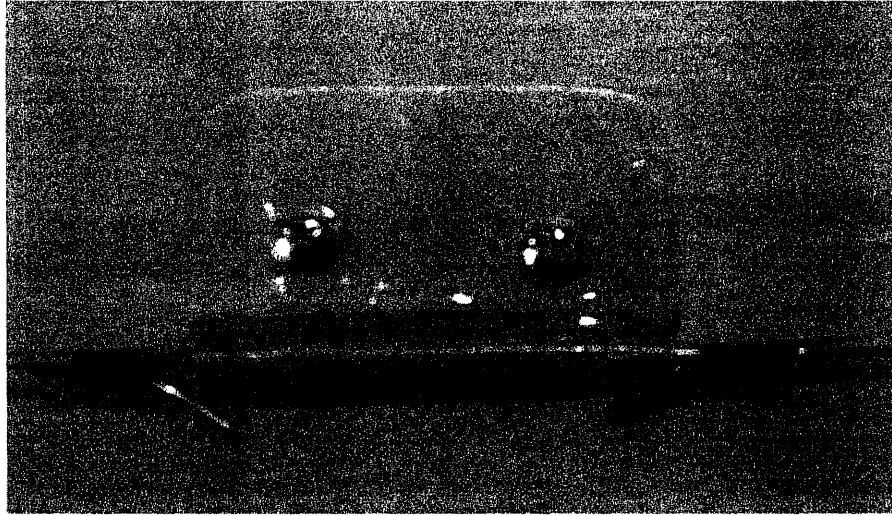
Figure 16: Photograph of hinge component (top view)

First, the welding rod was inserted through the tube. Then short welding rod protrusions were spot welded onto the inserted welding rod piece in a way so that the welding rod could pivot, but not slide out of the pivot. Also, the protrusions intersected with the free legs of the torsion springs, which provided resistance as mentioned above.

3.1.5 Support Frame

It was noted that the moment acting on the rim as the arm was forced closer to the solar concentrator would cause the rim to bend inward. In order to prevent this from happening, a support frame was built. Aluminum angle was used to build the support frame. It was cut into 3 pieces: 2 pieces that were 3.5" long and one piece that was 20" long. The ends of the pieces were cut at 45 degree angles, so they could joined by welding as shown in Figure 17.

Figure 17: Photograph of the support frame made out of aluminum angle

Another element was welded to the top of one of the sides of the support frame. This plate was 1/8" thick aluminum, and its other dimensions were 3" X 1.5". Two holes were drilled on this plate that matched the holes of the hinge component. The purpose of this was to allow for easy attachment of the hinge to the plate. A clamp on the opposite end was later added in order to stabilize the system.

4 Discussion and Conclusion

The tube design seemed to be a great idea theoretically, but after building a prototype of the design, it was found to be ineffective. The bicycle tire tube was not rigid enough to act as a key structural element. As a result, peeling occurred, and the solar concentrator could not be inflated to the point of equilibrium between the pressure inside of the bicycle tire tube and the pressure inside of the solar concentrator.

The rim design worked great utilizing a bandsaw blade (without teeth) as its structural element. The rim helped ease the radial stresses that the seal would otherwise have to completely incur. Bending of the rim made it less compact than the tube design was able to achieve, but it was still significant with a 2 to 1 ratio of fully expanded solar concentrator to compacted solar concentrator.

Figure 18 shows the difference in optical quality between the tube design and the rim design. It is evident that the rim design achieved a higher quality of reflection.
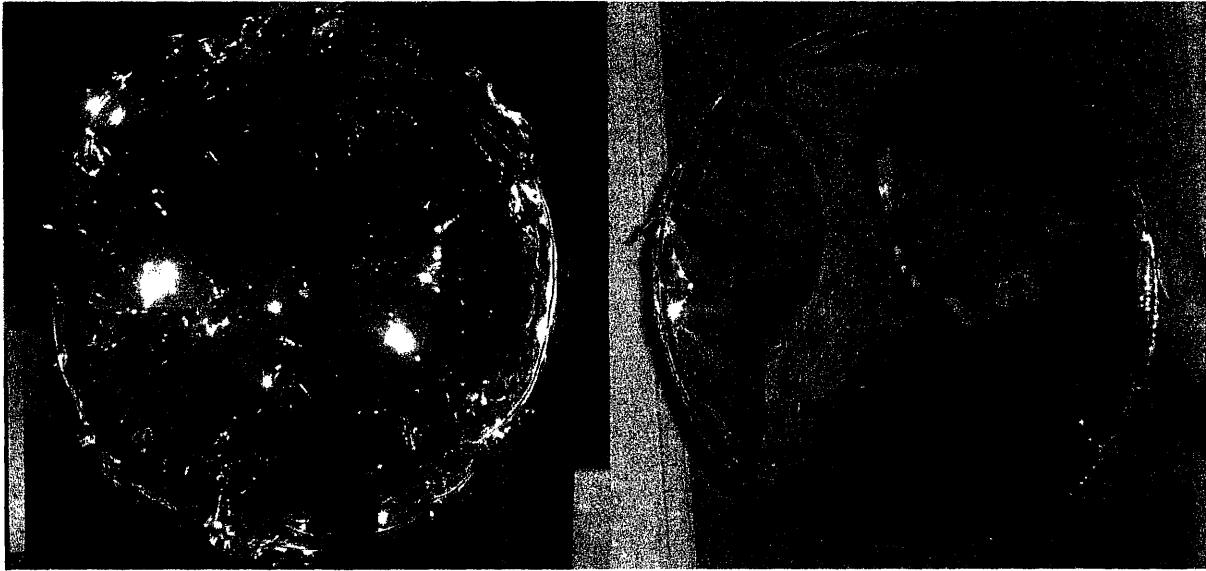
Figure 18: Comparison of reflection quality between tube design (left) and rim design (right)

This project still needs further work, due to the time frame and resources available.

It is suggested to attempt a sewing approach to sealing the system. Hand sewing around the rim could provide a strong bond between the two sheets of Mylar. Once sewn, the tiny holes created by the sewing could be sealed with Krazy glue or epoxy.

Another improvement that could be made is using the material Kapton instead of Mylar. Kapton may be a better option than Mylar because of it degrading less with UV radiation. Properties of Kapton are included in Appendix B.

5 Appendices

5.1 Appendix A (Drawings)
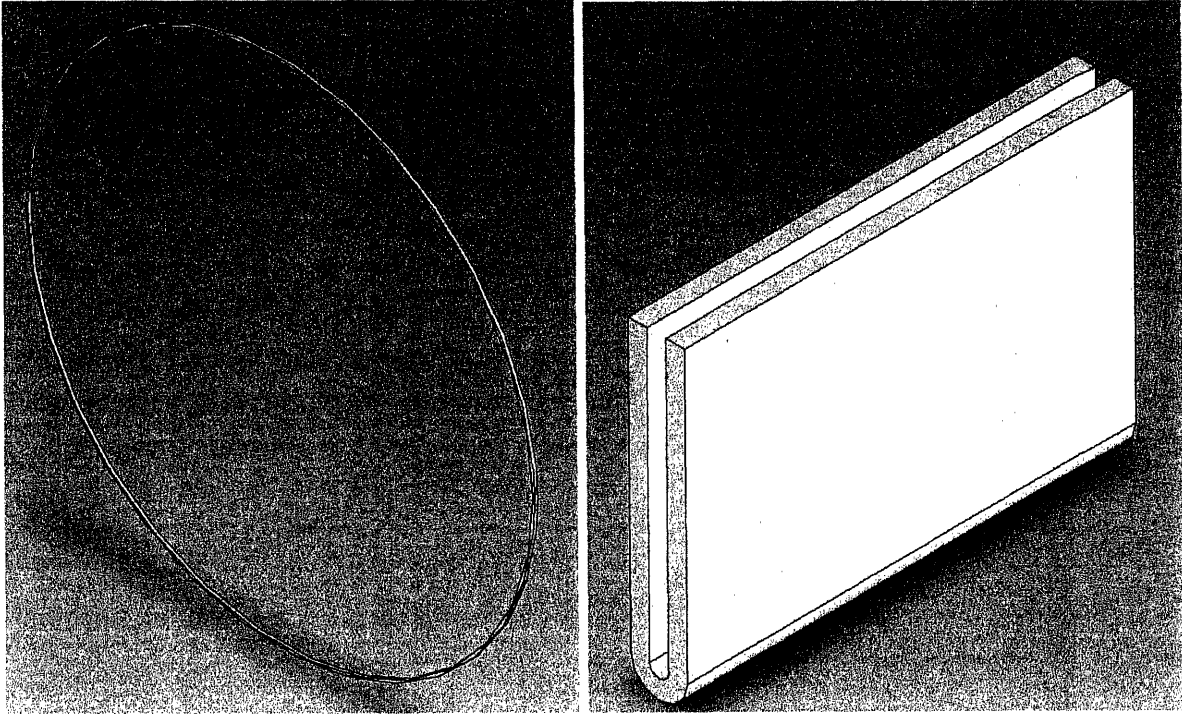
Solid models of rim and hinge components.

5.2 Appendix B   **(Provided by DuPont)**

Mylar®
polyester film

Introduction to Mylar® Polyester Films

Mylar® is a biaxially oriented, thermoplastic film made from ethylene glycol and dimethyl terephthalate (DMT).

Since DuPont first introduced Mylar® polyester film in the early 1950s, it has been used in a variety of applications that add value to products found in virtually all segments of the world economy. After more than 40 years, the future still holds great promise for Mylar®. Its excellent balance of properties and extraordinary range of performance capabilities make Mylar® ideal for a broad array of applications in the electrical/electronics, magnetic media, industrial specialty, imaging/graphics, and packaging markets.

Equally important to the versatility of Mylar® is its environmental friendliness. It is one of the most environmentally safe polymer products made today.

Mylar® polyester film, only by DuPont Teijin Films, is available uncoated or coated and in a broad variety of gauges and widths. We are committed to continually developing and improving our product offering. If you have an idea or a special need for a new film, we're ready to explore the possibilities. Just speak with your DuPont Teijin Films sales representative or give us a call at (800) 635-4639.

Balance of Properties

Mylar® polyester films have a unique combination of **physical, chemical, thermal, and optical** properties:

- **Strong, tough, brilliant, and clear.**
- **Ease of converting:**
  laminating, extrusion coating, embossing, metallizing, printing, punching, corrugation, dyeing, stamping or forming.
- **Ease of handling on high-speed equipment.**
- **Retain mechanical properties:**
  stiffness, strength, toughness, dimensional stability, and optical clarity, over an exceedingly wide range of temperatures.
- **Excellent temperature resistance.**
- **Readily combined with other materials.**
- **Strong tear-initiation and puncture resistance.**
- **Excellent oil, grease, or moisture barrier resistance.**
- **Excellent chemical resistance.**

How Mylar® Is Made (Figure 1)

- Molten polyethylene terephthalate (PET) polymer is first extruded onto a chill roll drum to form a film. ❶

- This film then is biaxially oriented by being stretched first in the machine direction (MD) ❷ and then in the transverse direction (TD).

- The orientation is accomplished by passing the film over rollers ❸ that run at increasingly faster speeds (MD orientation), then fed into a tenter frame, where it is pulled at right angles (TD orientation). This stretching rearranges the PET molecules into an orderly structure to substantially improve the film's mechanical properties. (Films stretched in the machine direction only are uniaxially oriented; films stretched in both directions are biaxially oriented.)

- Finally, the film is heat-set ❹ to stabilize it. It will not shrink again until exposed to its original heat-set temperature.

Figure 1. A Typical Manufacturing Process for Oriented Polyester Film
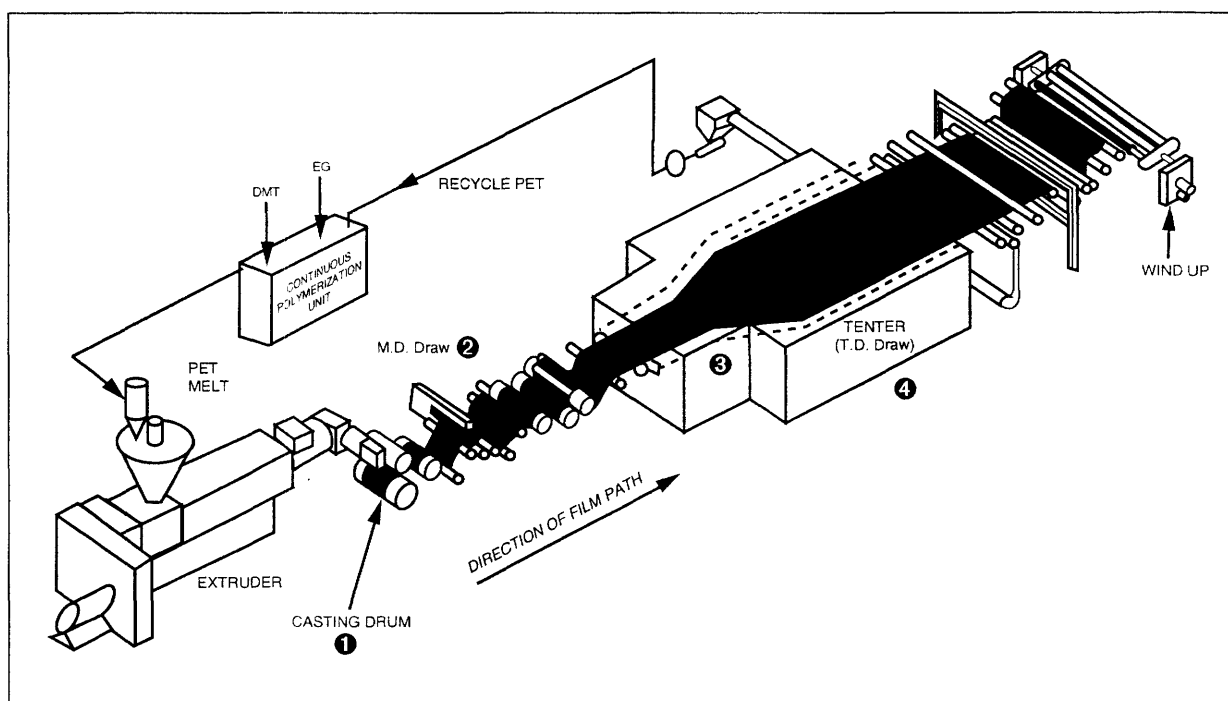
Mylar®

polyester film

Physical-Thermal Properties

Mylar® polyester film retains good physical properties over a wide temperature range (–70 to 150°C [–94 to 302°F]), and it is also used at temperatures from –250 to 200°C (–418 to 392°F) when the physical requirements are not as demanding.

Some physical and thermal properties of Mylar® are summarized in **Table 1**. Detailed information and other physical and thermal properties are described in the remaining pages of this bulletin.

Table 1
Typical Physical and Thermal Properties of Mylar® Polyester Film

Property	Typical Value	Unit	Test Method
Gauge and Type End Use	92A Industrial		

Ultimate Tensile
  Strength, MD
          TD
	20 (29)
	24 (34)
		kg/mm² (kpsi)	ASTM D 882

Strength at 5%
  Elongation (F-5), MD
             TD
	10 (15)
	10 (14)
		kg/mm² (kpsi)	ASTM D 882

Modulus, MD TD	490 (710) 510 (740)	kg/mm² (kpsi)	ASTM D 882
Elongation, MD TD	116 91	%	ASTM D 882
Surface Roughness Ra	38	nm	Optical profilometer
Density	1.390	g/cm³	ASTM D 1505
Viscosity	0.56		ASTM D 2857
Melt Point	254	°C	DSC*

Dimensional Stability
  at 105°C (221°F), MD
               TD
  at 150°C (302°F), MD
               TD
	0.6
	0.9
	1.8
	1.1
		%	DuPont test

Specific Heat	0.28	cal/g/°C	

Coefficients of
  Thermal Expansion
  Thermal Conductivity
  (Mylar® 1000A)
	1.7×10^{-5}
	3.7×10^{-4}
		in/in/°C
		$\dfrac{cal \cdot cm}{cm^2 \cdot sec \cdot °C}$
			ASTM D 696
			30–50°C (86–122°F)
			25–75°C (77–167°F)

UL94 Flame Class	See UL file # E93687	VTM	

*Differential Scanning Calorimeter

Tensile Properties

Figure 1 shows typical stress-strain curves for Mylar® polyester film at various temperatures. Poisson's ratio is typically 0.38 before yield and 0.58 after yield.

Figure 1.   Stress-Strain Curves
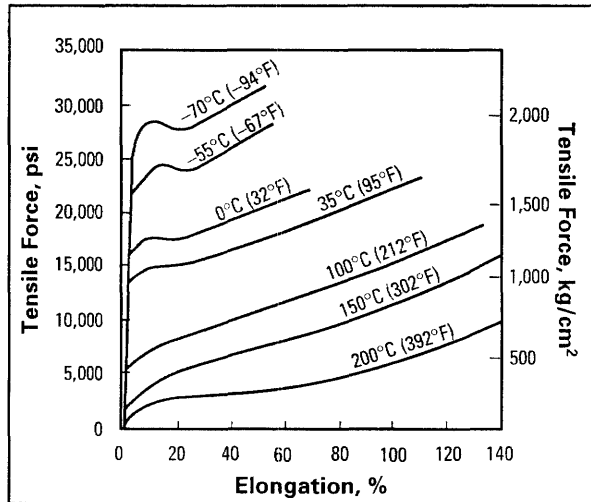
Temperature affects the tensile properties of Mylar®; data on a typical sample are shown in **Figure 2**. When considering the use of Mylar® at high temperatures, reference should be made to the last five pages of this bulletin.

Figure 2.   Tensile Properties vs. Temperature
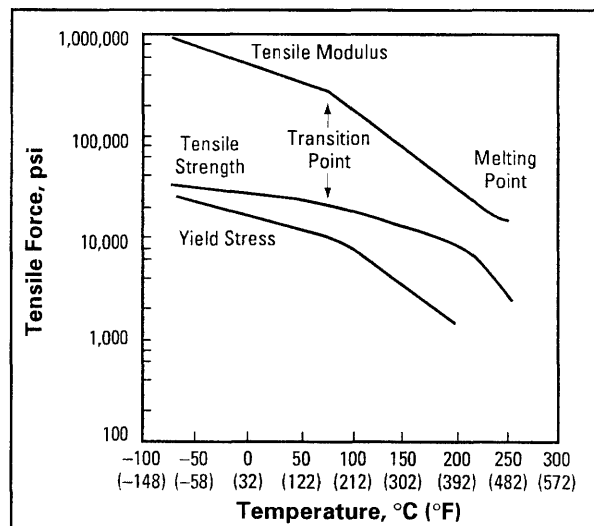
Compressive Properties

Compression tests provide information about the compressive properties of plastics when employed under relatively low uniform rates of uniaxially applied loading. Data on the compressive properties of Mylar® polyester film were obtained in accordance with ASTM D 695, except that a cylindrical pile of pieces 1 in high, 1 in in diameter, was used. The data are summarized in **Table 2**.

When loaded in compression, Mylar® did not exhibit a yield point nor did it fail in compression by a shattering fracture. Therefore, it would be inappropriate to report any value as a compressive strength. However, the stress at 2% deformation and the stress at 1% offset have been calculated. Because the latter stress occurs at very nearly the point where the stress-strain curve begins to deviate markedly from the initial relatively linear portion, it is probably a meaningful upper limit for any application where Mylar® is loaded in compression.

Shear Strength

Mylar® has a shear strength that is significantly higher than published data for other polymeric materials such as acetals, nylons, and polyolefins. Shear strength was measured by a punch-type of test according to ASTM D 732 and is reported in the pounds of force to shear divided by the product of the circumference and the thickness. These tests showed that 5 and 10 mil Mylar® films have shear strengths of 15.0 (21.5) and 13.6 (19.5) kg/mm² (kpsi), respectively.

Dimensional Stability

The main factors affecting dimensional stability of film are strain relief, thermal expansion, hygroscopic expansion, and creep. Typical values for these factors are described on following pages.

Strain Relief

Strain relief (also called residual shrinkage) occurs when a film is heated to an elevated temperature. The resulting shrinkage of the film is merely a relaxation of strains induced during the manufacture of the film or during processing of the film. Once these strains are relieved at a specific temperature, there should be no further shrinkage due to strain relief as long as that temperature is not reached.

Table 2
Compressive Properties of Mylar® Polyester Film

Film Type	Compressive Modulus, kg/mm² (kpsi)	Stress, kg/mm² (kpsi) at 2% Deformation	1% Offset Stress, kg/mm² (kpsi)	Maximum Stress During Test, kg/mm² (kpsi)	Maximum Strain During Test, %
Mylar® 1000A	289 (413)	5.91 (8.45)	11.8 (16.8)	21 (30)	23
Mylar® 1400A	278 (397)	5.76 (8.23)	11.6 (16.6)	21 (30)	27

Some typical curves of shrinkage due to strain relief are shown in **Figures 3** and **4** for two types of Mylar® polyester film.
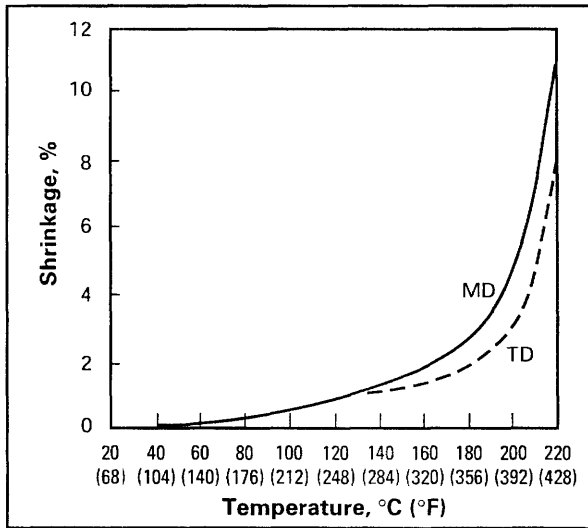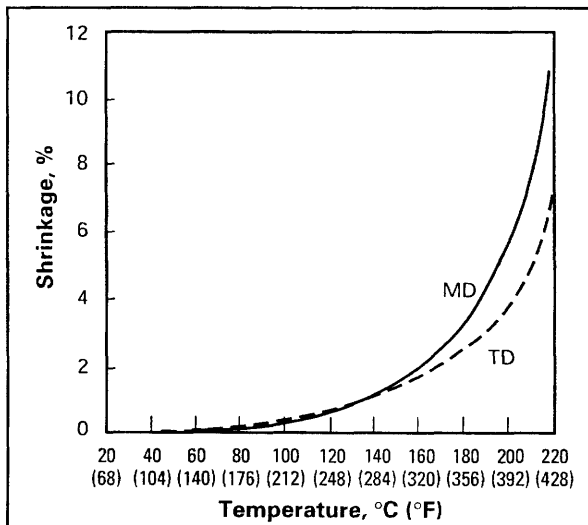
Figure 3. Shrinkage vs. Temperature—Mylar® 92A

Figure 4. Shrinkage vs. Temperature—Mylar® 750A

Thermal Expansion

The thermal coefficient of linear expansion of Mylar® is 1.7×10^{-5} in/in/°C (9.5×10^{-6} in/in/°F). As a guide to estimating changes due to thermal expansion, **Figure 5** gives the dimensional changes (in/in) over a wide temperature range. Multiplying the indicated change by the sample length gives the thermal dimensional change in the sheet of Mylar®.

Figure 5. Dimensional Stability vs. Temperature Changes
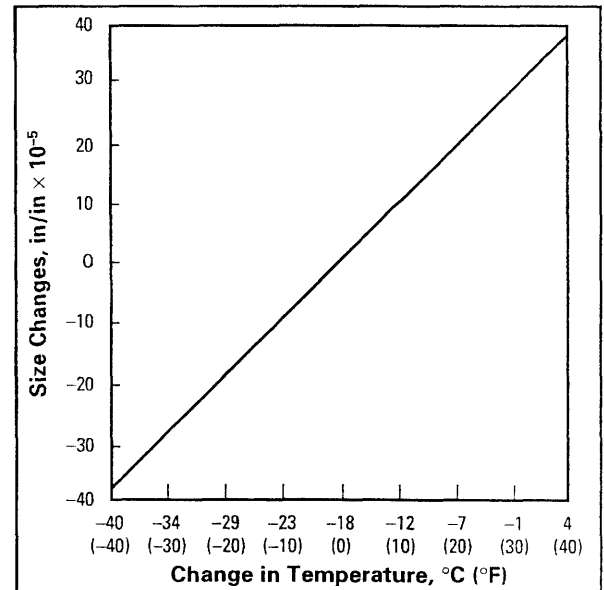
Hygroscopic Expansion

The hygroscopic coefficient of linear expansion is 0.6×10^{-5} in/in/% RH for Mylar® polyester film. The dimensional change due to hygroscopic expansion over a wide range of humidities is shown in **Figure 6**. To calculate the total dimensional change in a sheet of Mylar® due to hygroscopic expansion, multiply the indicated change by the linear dimensions of the sheet. Under normal atmospheric conditions, changes in thermal expansion tend to compensate for changes in hygroscopic expansion because rising temperatures usually result in lowering in the relative humidity.

**Figure 6. Dimensional Stability vs. Relative Humidity Changes**
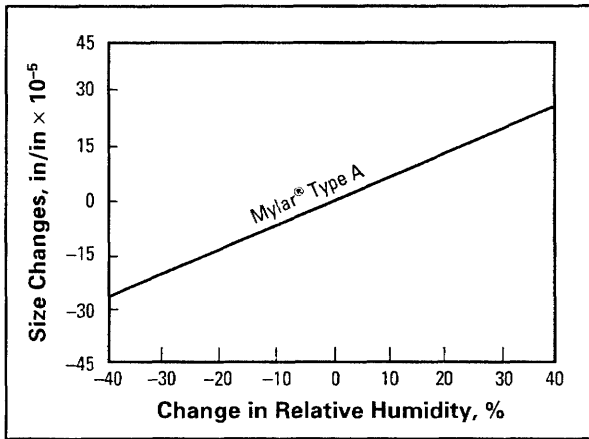
Creep

Mylar® is unusually resistant to creep. Two values measured at room temperature are 0.1% after 260 hr at 2.09 kg/mm² (2.98 kpsi) and 0.2% after 1000 hr at 2.10 kg/mm² (3.00 kpsi). After 4000 hr at 0.35 kg/mm² (0.50 kpsi) in 100°C (212°F) oven, a creep of 0.9% was measured.

Hydrolytic Stability

Mylar® polyester film will hydrolyze and become brittle under conditions of high temperature and humidity, as shown by the effect of steam on the tensile properties of Mylar® (**Figures 7, 8,** and **9**). Therefore, care should be taken to ensure that there is a minimum of water in any hermetically sealed unit. Adequate removal of water from Mylar® is usually obtained by heating for 4 hr at 160°C

Figure 7. Tensile Strength of Mylar® after Exposure to Steam
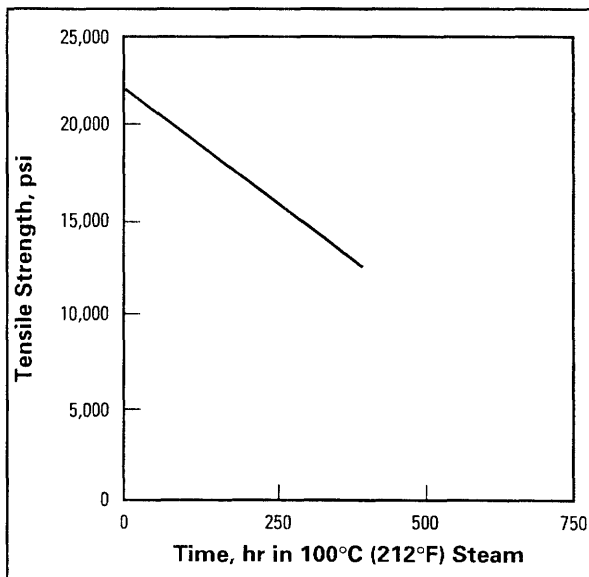
(320°F). (Drying at these conditions should reduce the water content of the film to less than 0.1%; more than this amount of water must be present in a system before the film can become embrittled due to hydrolysis.) Drying at lower temperatures is not as effective in removing water as shown in **Figure 10**. Data for this figure were obtained with samples of Mylar® 1000A conditioned for one month at 22°C (72°F) and 80% RH and then dried under vacuum for 4 hr at the indicated temperatures.

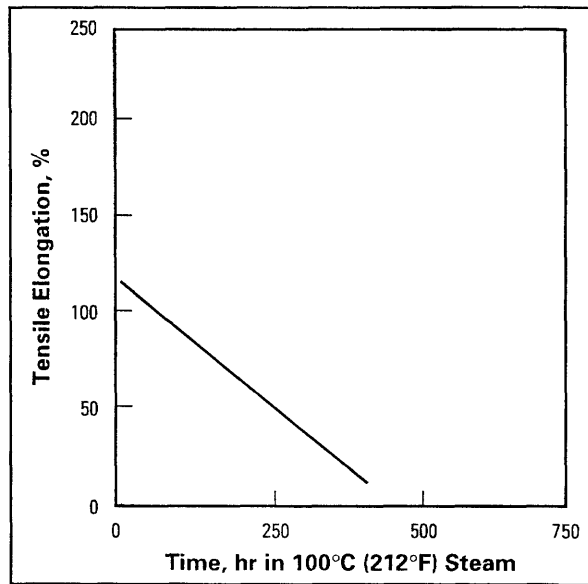**Figure 8. Tensile Elongation of Mylar® after Exposure to Steam**

Figure 9. Tensile Modulus of Mylar® after Exposure to Steam
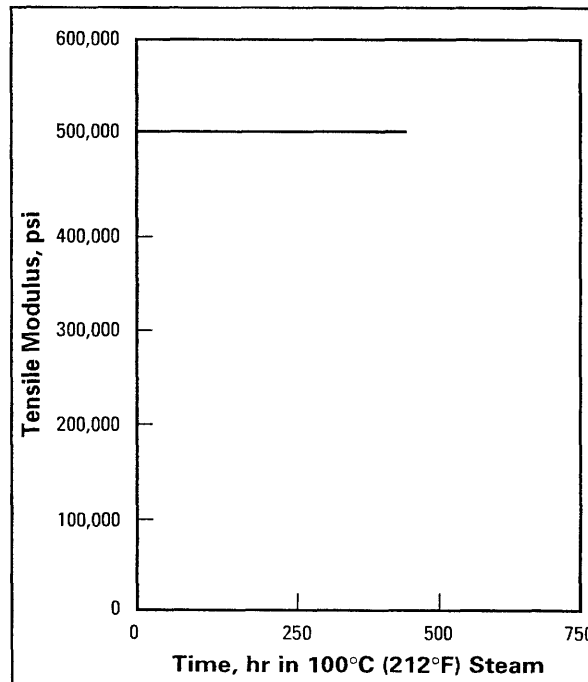

4   39

Figure 10. Effect of Temperature on the Removal of Water from Mylar®
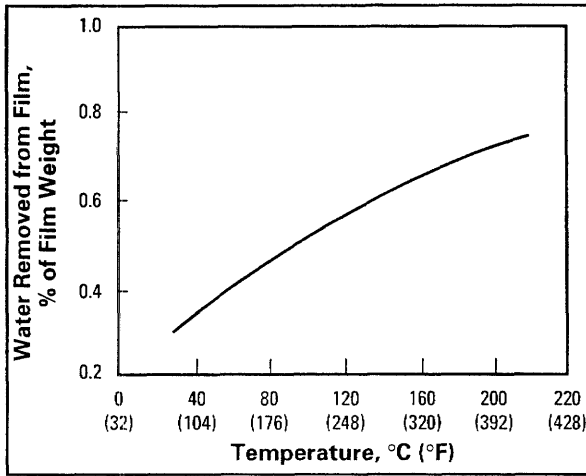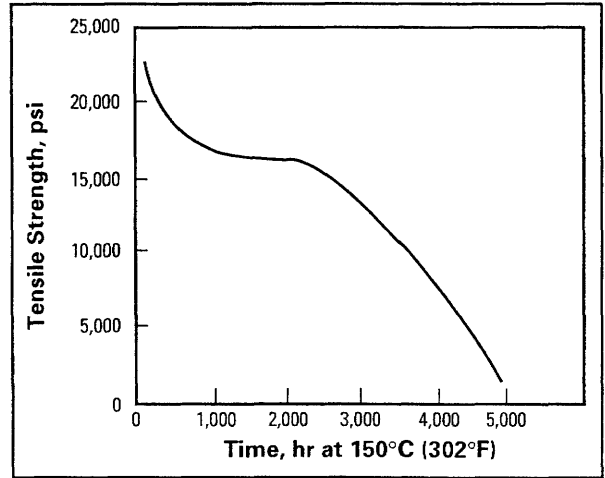

**Figure 11. Tensile Strength of Mylar® after Heating in 150°C (302°F) Air**

Heat Aging

The maximum service temperature usually recommended for Mylar® polyester film is 150°C (302°F). Where extensive exposure, severe environmental conditions, or unusual physical requirements are involved, it may be necessary to reduce service temperatures. However, coatings are available to increase the resistance of Mylar® to the effects of heat aging. The effects of heat aging on uncoated Mylar® in 150°C (302°F) air are shown in **Figures 11** and **12**.

Processing conditions for Mylar® should be kept below 200°C (392°F) to prevent damaging the film. For instance, if heated at 220°C (428°F) for 30 min, the film loses about 10% of its tensile strength; moreover, the film becomes brittle and shatters after heating at 235°C (455°F) for less than 1 min.
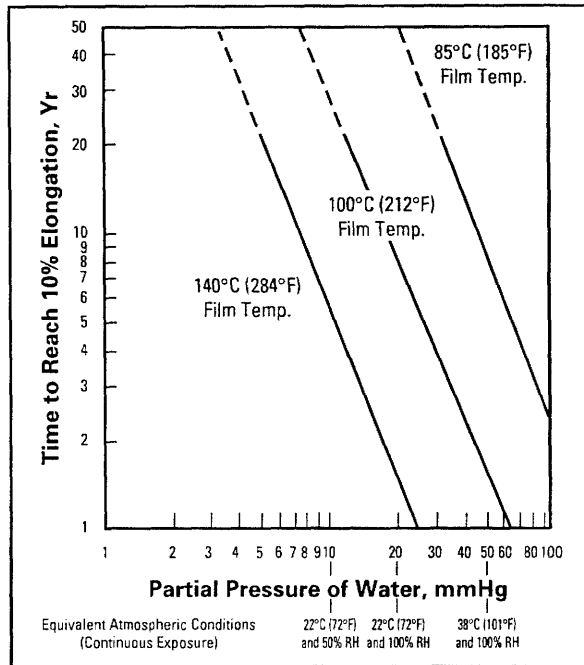
Figure 12. Tensile Elongation of Mylar® after Heating in 150°C (302°F) Air

40   5
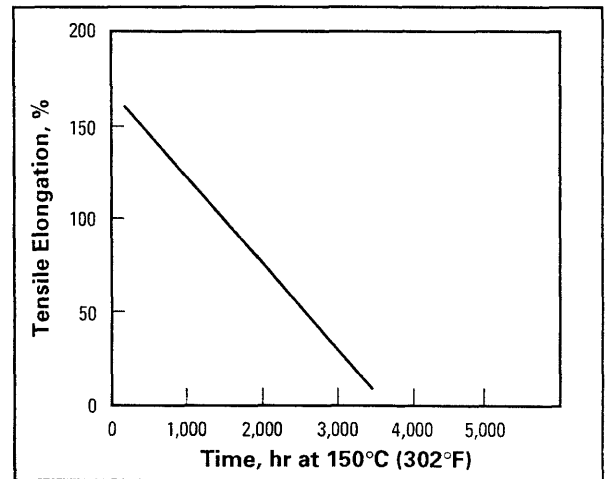
Service Life

The service life of Mylar®, when subject to severe flexing, is considered to be the time required to reach 10% elongation under various conditions of humidity and operating temperature. The curves shown in **Figure 13** are based upon tests of Mylar® 92 and 1000A at various partial pressures of water. The estimated service life will be greater when the film is suitably encapsulated or coated. Longer life can also be expected when the Mylar® is not subject to flexing.

Figure 13. Effect of the Partial Pressure of Water on Service Life

Mylar®
Only by DuPont Teijin Films

Permeability

Mylar® polyester film is virtually impermeable to the liquid phase of most chemicals and reagents. The permeability of Mylar® to the vapor phase of some typical chemicals is shown in **Table 4**. The effect of film thickness on the rate of water vapor transmission through Mylar® is shown in **Figure 1**. Gas permeability rates are shown in **Table 4** and **Figure 2**. Marked reductions in gas permeability (up to a factor of 100) can be obtained through polymeric coatings, metal foil laminations, or vacuum metallization.

Table 4
Permeability of Mylar® to Gases and Vapors

Vapors	g/100 in²/24 hr/mil*
Acetone	2.22
Benzene	0.36
Carbon Tetrachloride	0.08
Ethyl Acetate	0.08
Hexane	0.12

Gas	Temp., °C (°F)	cc/100 in²/ 24 hr/atm/mil	Test Method
Carbon Dioxide	25 (77)	16	ASTM D1434-58
Freon® 12	55 (131)	0.01	
Methane	25 (77)	1	

* Permeabilities of vapors are determined at the vapor pressure of the liquid at the temperature of the test, 40°C (104°F), using 1 mil film.

Figure 1. Water Vapor Transmission Rate of Mylar® at 38°C (100°F) (ASTM E-96, Procedure E)
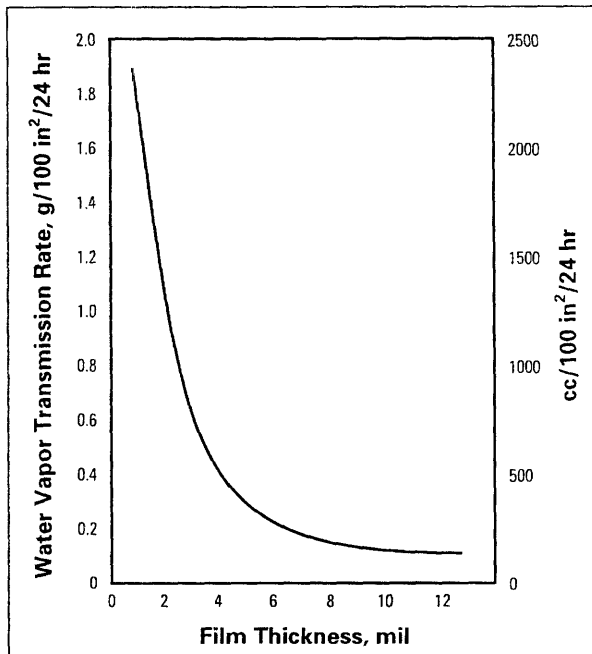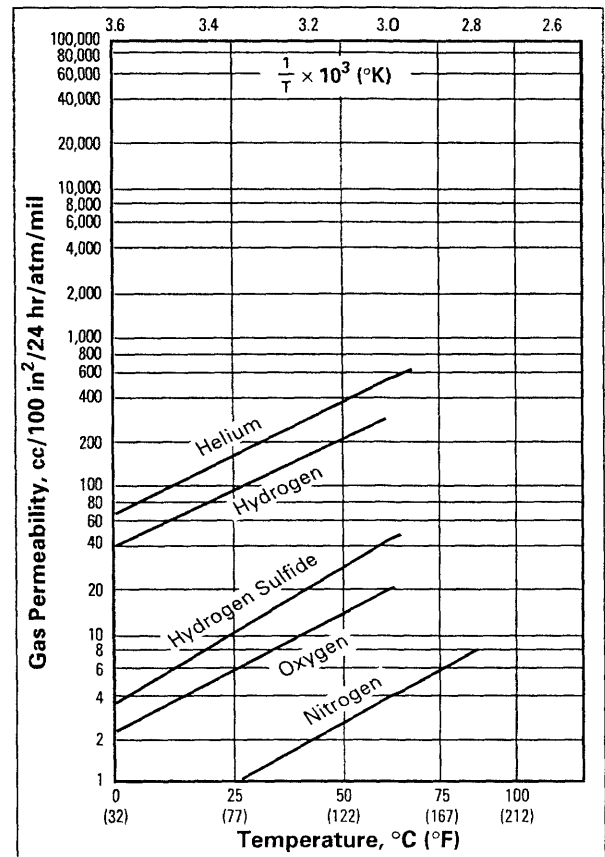

Figure 2. Gas Permeability of Mylar® vs. Temperature

Moisture Absorption

Mylar® polyester film is relatively insensitive to moisture absorption. It absorbs less than 0.8% moisture when totally immersed in water for 24 hr (ASTM D-570-63). For sheet samples hanging in air, with a relative humidity of 80%, the time required to absorb moisture increases as the film thickness increases (see **Table 5**). The effect of relative humidity on the moisture content of single sheet samples is shown in **Figure 3**. (Moisture content was determined by drying at 100°C (212°F) —drying at 150°C (302°F) drives off another 0.2 to 0.3% water.)

For slit rolls of film, the rate of change in moisture content of Mylar® is very slow because of the low moisture permeability of the film. Hence, except for very unusual situations, the moisture content of the film at the time of manufacture will be maintained until processed by the customer.

Table 5
Rate of Moisture Gain of Single Sheets of Mylar®

Gauge, mil	Time Required to Gain 90% Equilibrium Moisture Content, min
½	15
1	60
5	135

Kapton® polyimide film possesses a unique combination of properties that make it ideal for a variety of applications in many different industries. The ability of Kapton® to maintain its excellent physical, electrical, and mechanical properties over a wide temperature range has opened new design and application areas to plastic films.

Kapton® is synthesized by polymerizing an aromatic dianhydride and an aromatic diamine. It has excellent chemical resistance; there are no known organic solvents for the film. Kapton® does not melt or burn as it has the highest UL-94 flammability rating: V-0. The outstanding properties of Kapton® permit it to be used at both high and low temperature extremes where other organic polymeric materials would not be functional.

Adhesives are available for bonding Kapton® to itself and to metals, various paper types, and other films.

Kapton® polyimide film can be used in a variety of electrical and electronic insulation applications: wire and cable tapes, formed coil insulation, substrates for flexible printed circuits, motor slot liners, magnet wire insulation, transformer and capacitor insulation, magnetic and pressure-sensitive tapes, and tubing. Many of these applications are based on the excellent balance of electrical, thermal, mechanical, physical, and chemical properties of Kapton® over a wide range of temperatures. It is this combination of useful properties at temperature extremes that makes Kapton® a unique industrial material.

Three types of Kapton® are described in this bulletin:

- Kapton® Type HN, all-polyimide film, has been used successfully in applications at temperatures as low as -269°C (-452°F) and as high as 400°C (752°F).

Type HN film can be laminated, metallized, punched, formed, or adhesive coated. It is available as 7.5 μm (0.3 mil), 12.5 μm (0.5 mil), 19 μm (0.75 mil), 25 μm (1 mil), 50 μm (2 mil), 75 μm (3 mil), and 125 μm (5 mil) films.

- Kapton® Type VN, all-polyimide film with all of the properties of Type HN, plus superior dimensional stability. Type VN is available as 12.5 μm (0.5 mil), 19 μm (0.75 mil), 25 μm (1 mil), 50 μm (2 mil), 75 μm (3 mil), and 125 μm (5 mil) films.

- Kapton® Type FN, a Type HN film coated on one or both sides with Teflon® FEP fluoropolymer resin, imparts heat sealability, provides a moisture barrier, and enhances chemical resistance. Type FN is available in a number of combinations of polyimide and Teflon® FEP thicknesses (see Table 16).

Note: In addition to these three types of Kapton®, films are available with the following attributes:

- antistat
- thermally conductive
- polyimides for fine line circuitry
- cryogenic insulation
- corona resistant
- pigmented for color
- conformable
- other films tailored to meet customers' needs

Data for these films are covered in separate product bulletins, which can be obtained from your DuPont representative.

The Chemical Abstracts Service Registry Number for Kapton® polyimide film is [25036-53-7].

1
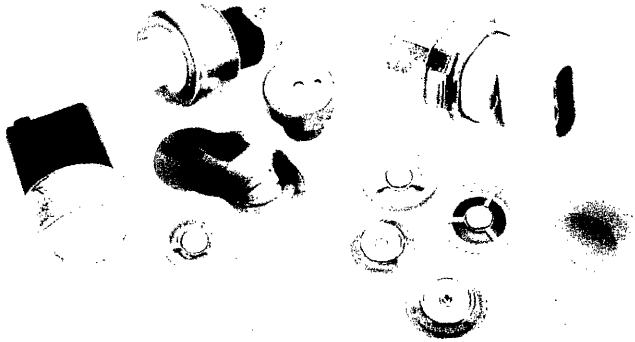
Kapton® withstands the harsh chemical and physical demands on diaphragms used in automotive switches.
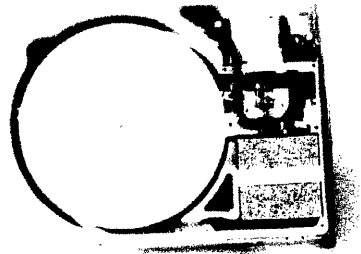
Kapton® is used in numerous electronic applications, including hard disk drives.

2

Kapton® polyimide films retain their physical properties over a wide temperature range. They have been used in field applications where the environmental temperatures were as low as −269°C (−452°F) and as high as 400°C (752°F). Complete data are not available at these extreme conditions, and the majority of technical data presented in this section falls in the 23 to 200°C (73 to 392°F) range.

Table 1
Physical Properties of Kapton® Type 100 HN Film, 25 μm (1 mil)

Physical Property	Typical Value at 23°C (73°F)	Typical Value at 200°C (392°F)	Test Method
Ultimate Tensile Strength, MPa (psi)	231 (33,500)	139 (20,000)	ASTM D-882-91, Method A*
Yield Point at 3%, MPa (psi)	69 (10,000)	41 (6000)	ASTM D-882-91
Stress to Produce 5% Elongation, MPa (psi)	90 (13,000)	61 (9000)	ASTM D-882-91
Ultimate Elongation, %	72	83	ASTM D-882-91
Tensile Modulus, GPa (psi)	2.5 (370,000)	2.0 (290,000)	ASTM D-882-91
Impact Strength, N·cm (ft·lb)	78 (0.58)		DuPont Pneumatic Impact Test
Folding Endurance (MIT), cycles	285,000		ASTM D-2176-89
Tear Strength—Propagating (Elmendorf), N (lbf)	0.07 (0.02)		ASTM D-1922-89
Tear Strength—Initial (Graves), N (lbf)	7.2 (1.6)		ASTM D-1004-90
Density, g/cc or g/mL	1.42		ASTM D-1505-90
Coefficient of Friction—Kinetic (Film-to-Film)	0.48		ASTM D-1894-90
Coefficient of Friction—Static (Film-to-Film)	0.63		ASTM D-1894-90
Refractive Index (Sodium D Line)	1.70		ASTM D-542-90
Poisson's Ratio	0.34		Avg. Three Samples Elongated at 5%, 7%, 10%
Low Temperature Flex Life	Pass		IPC TM 650, Method 2.6.18

*Specimen Size: 25 × 150 mm (1 × 6 in); Jaw Separation: 100 mm (4 in); Jaw Speed: 50 mm/min (2 in/min); Ultimate refers to the tensile strength and elongation measured at break.

Table 2
Thermal Properties of Kapton® Type 100 HN Film, 25 μm (1 mil)

Thermal Property	Typical Value	Test Condition	Test Method
Melting Point	None	None	ASTM E-794-85 (1989)
Thermal Coefficient of Linear Expansion	20 ppm/°C (11 ppm/°F)	−14 to 38°C (7 to 100°F)	ASTM D-696-91
Coefficient of Thermal Conductivity, W/m·K	0.12	296 K	ASTM F-433-77 (1987)[1]
$\frac{cal}{cm\cdot sec\cdot°C}$	2.87×10^{-4}	23°C	
Specific Heat, J/g·K (cal/g·°C)	1.09 (0.261)		Differential Calorimetry
Flammability	94V-0		UL-94 (2-8-85)
Shrinkage, %	0.17 1.25	30 min at 150°C 120 min at 400°C	IPC TM 650, Method 2.2.4A ASTM D-5214-91
Heat Sealability	Not Heat Sealable		
Limiting Oxygen Index, %	37		ASTM D-2863-87
Solder Float	Pass		IPC TM 650, Method 2.4.13A
Smoke Generation	DM = <1	NBS Smoke Chamber	NFPA-258
Glass Transition Temperature (T$_g$)	A second order transition occurs in Kapton® between 360°C (680°F) and 410°C (770°F) and is assumed to be the glass transition temperature. Different measurement techniques produce different results within the above temperature range.		

3

Table 3
Physical and Thermal Properties of Kapton® Type VN Film

Property	Typical Value for Film Thickness				Test Method
	25 μm (1 mil)	50 μm (2 mil)	75 μm (3 mil)	125 μm (5 mil)	
Ultimate Tensile Strength, MPa (psi)	231 (33,500)	234 (34,000)	231 (33,500)	231 (33,500)	ASTM D-882-91
Ultimate Elongation, %	72	82	82	82	ASTM D-882-91
Tear Strength—Propagating (Elmendorf), N	0.07	0.21	0.38	0.58	ASTM D-1922-89
Tear Strength—Initial (Graves), N	7.2	16.3	26.3	46.9	ASTM D-1004-90
Folding Endurance (MIT), × 10³ cycles	285	55	6	5	ASTM D-2176-89
Density, g/cc or g/mL	1.42	1.42	1.42	1.42	ASTM D-1505-90
Flammability	94V-0	94V-0	94V-0	94V-0	UL-94 (2-8-85)
Shrinkage, %, 30 min at 150°C (302°F)	0.03	0.03	0.03	0.03	IPC TM 650 Method 2.2.4A
Limiting Oxygen Index, %	37	43	46	45	ASTM D-2863-87

Table 4
Physical Properties of Kapton® Type FN Film*

Property	Typical Value for Film Type**		
	120FN616	150FN019	250FN029
Ultimate Tensile Strength, MPa (psi)			
23°C (73°F)	207 (30,000)	162 (23,500)	200 (29,000)
200°C (392°F)	121 (17,500)	89 (13,000)	115 (17,000)
Yield Point at 3%, MPa (psi)			
23°C (73°F)	61 (9000)	49 (7000)	58 (8500)
200°C (392°F)	42 (6000)	43 (6000)	36 (5000)
Stress at 5% Elongation, MPa (psi)			
23°C (73°F)	79 (11,500)	65 (9,500)	76 (11,000)
200°C (392°F)	53 (8000)	41 (6000)	48 (7000)
Ultimate Elongation, %			
23°C (73°F)	75	70	85
200°C (392°F)	80	75	110
Tensile Modulus, GPa (psi)			
23°C (73°F)	2.48 (360,000)	2.28 (330,000)	2.62 (380,000)
200°C (392°F)	1.62 (235,000)	1.14 (165,000)	1.38 (200,000)
Impact Strength at 23°C (73°F), N·cm (ft·lb)	78 (0.58)	68.6 (0.51)	156.8 (1.16)
Tear Strength—Propagating (Elmendorf), N (lbf)	0.08 (0.02)	0.47 (0.11)	0.57 (0.13)
Tear Strength—Initial (Graves), N (lbf)	11.8 (2.6)	11.5 (2.6)	17.8 (4.0)
Polyimide, wt%	80	57	73
FEP, wt%	20	43	27
Density, g/cc or g/mL	1.53	1.67	1.57

*Test methods for **Table 4** are the same as for **Table 1**.

**Because a number of combinations of polyimide film and fluorocarbon coating add up to the same total gauge, it is necessary to distinguish among them. A three-digit system is used in which the middle digit represents the nominal thickness of the base Kapton® film in mils. The first and third digits represent the nominal thickness of the coating of Teflon® FEP fluoropolymer resin in mils. The symbol 9 is used to represent 13 μm (0.5 mil) and 6 to represent 2.5 μm (0.1 mil). Example: 120FN616 is a 120-gauge structure consisting of a 25 μm (1 mil) base film with a 2.5 μm (0.1 mil) coating of Teflon® on each side.

4

The usual values of tensile strength, tensile modulus, and ultimate elongation at various temperatures can be obtained from the typical stress–strain curves shown in **Figures 1** and **2**. Such properties as tensile strength and modulus are inversely proportional to temperature, whereas elongation reaches a maximum value at about 300°C (570°F). Other factors, such as humidity, film thickness, and tensile elongation rates, were found to have only a negligible effect on the shape of the 23°C (73°F) curve.

Figure 1. Tensile Stress–Strain Curves, Type HN Film, 25 μm (1 mil)
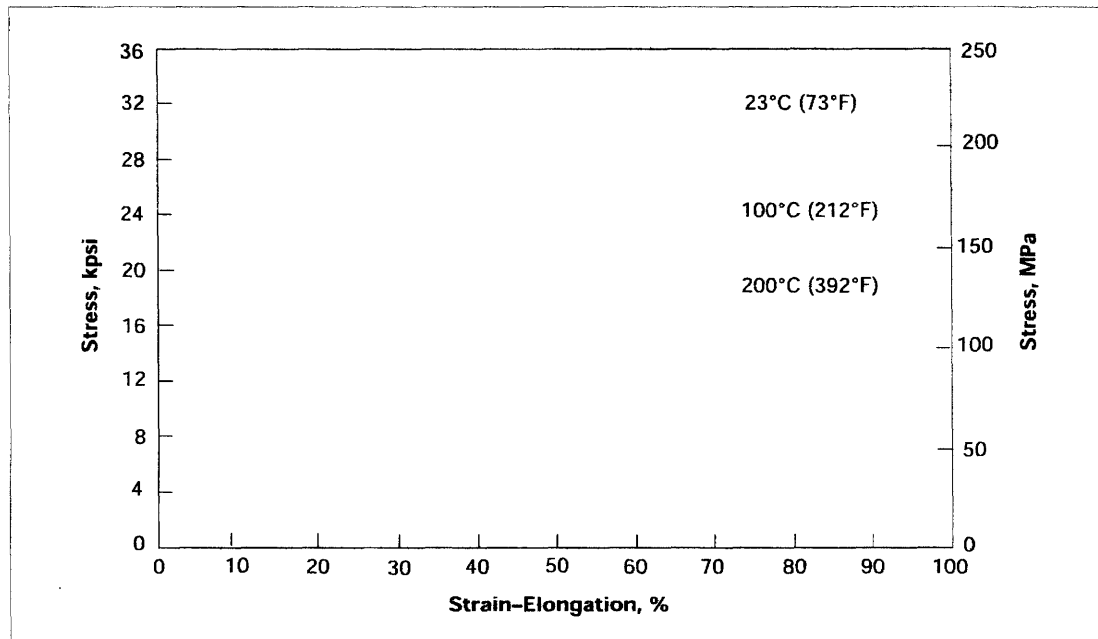
Figure 2. Tensile Creep Properties, Type HN Film, 25 μm (1 mil)

5
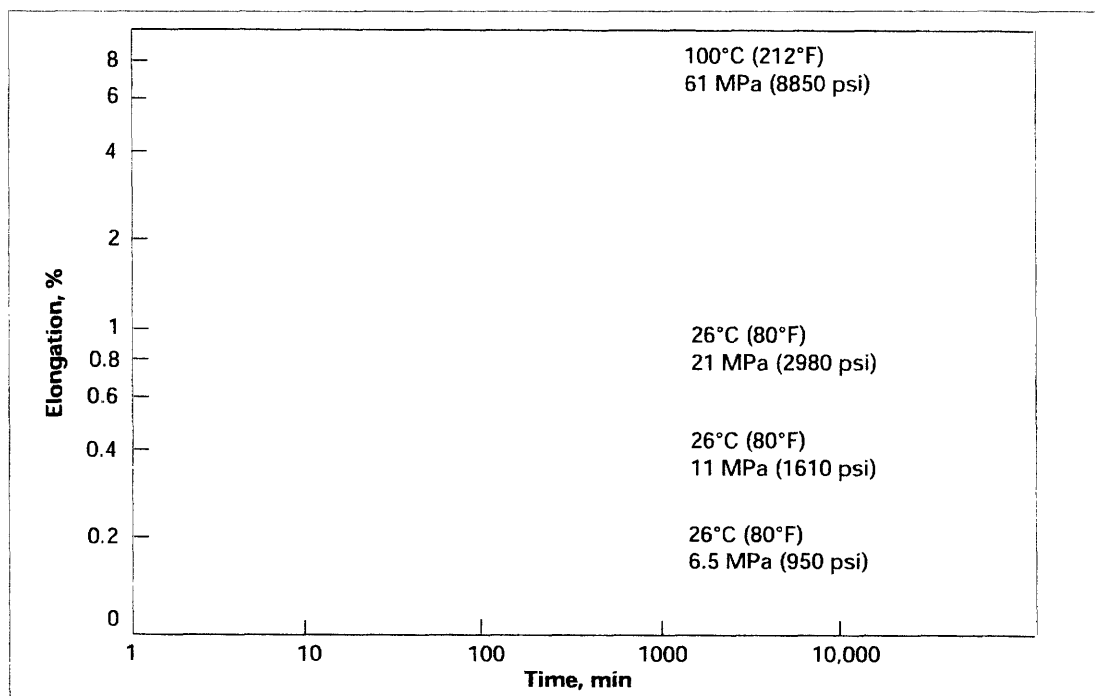
Kapton® polyimide film is made by a condensation reaction; therefore, its properties are affected by water. Although long-term exposure to boiling water, as shown in the curves in **Figures 3** and **4**, will reduce the level of film properties, sufficient tensile and elongation remain to ensure good mechanical performance. A decrease in the temperature and the water content will reduce the rate of Kapton® property reduction, whereas higher temperature and pressure will increase it.

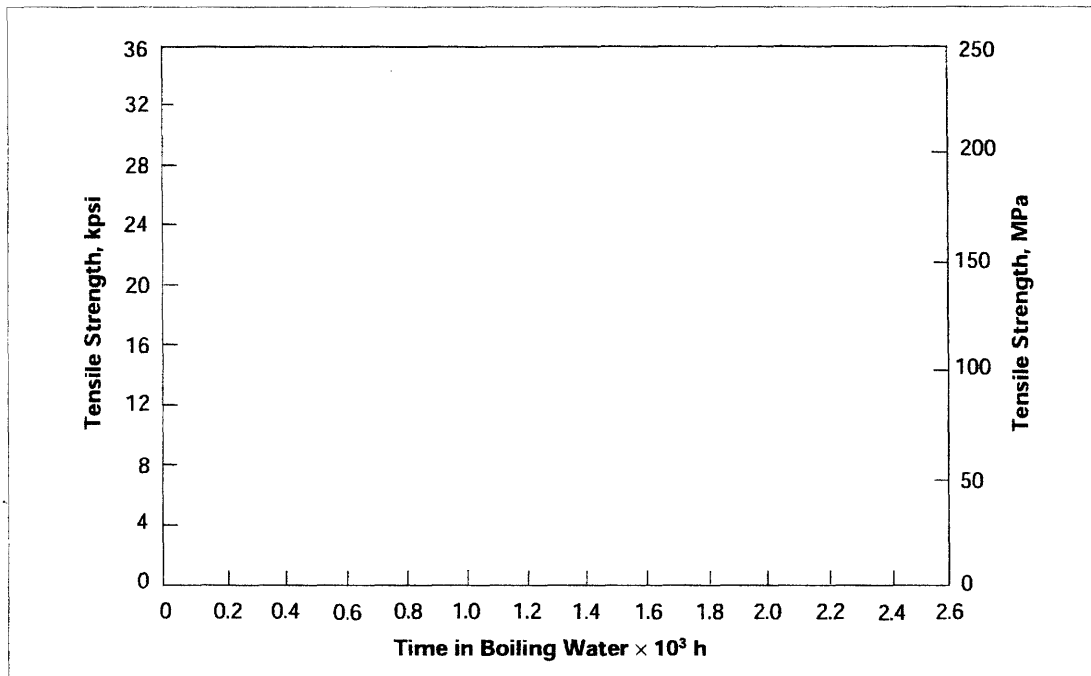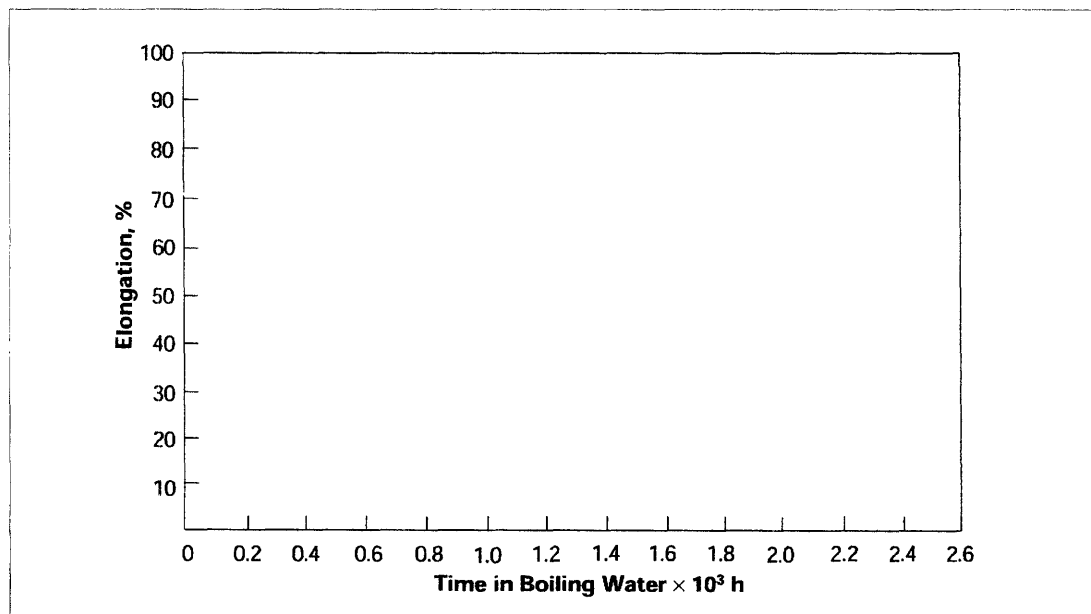**Figure 3. Tensile Strength After Exposure to 100°C (212°F) Water, Type HN Film, 25 μm (1 mil)**

Figure 4. Ultimate Elongation After Exposure to 100°C (212°F) Water, Type HN Film, 25 μm (1 mil)

6

The dimensional stability of Kapton® polyimide film depends on two factors—the normal coefficient of thermal expansion and the residual stresses placed in the film during manufacture. The latter causes Kapton® to shrink on its first exposure to elevated temperatures as indicated in the bar graph in **Figure 5**. Once the film has been exposed, the normal values for the thermal coefficient of linear expansion as shown in **Table 5** can be expected.

Figure 5. Residual Shrinkage vs. Exposure Temperature and Thickness, Type HN and VN Films
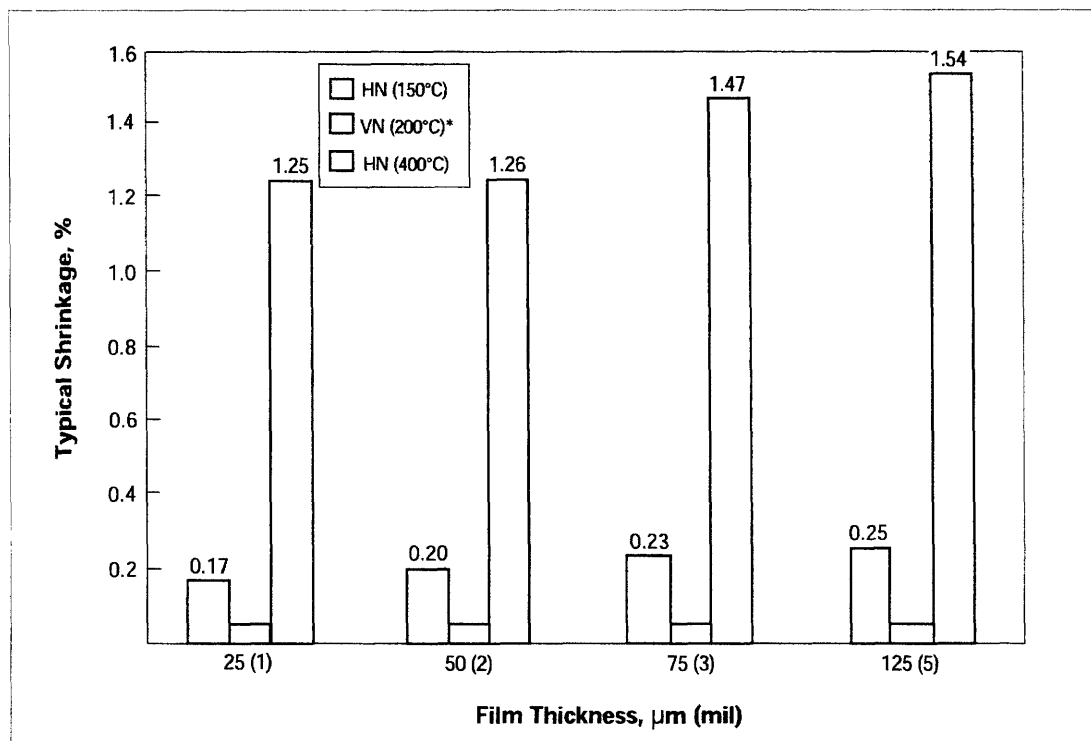
*Type VN shrinkage is 0.03% for all thicknesses.

Table 5
Thermal Coefficient of Expansion,
Type HN Film, 25 μm (1 mil),
Thermally Exposed

Temperature Range, °C (°F)	ppm/°C
30–100 (86–212)	17
100–200 (212–392)	32
200–300 (392–572)	40
300–400 (572–752)	44
30–400 (86–752)	34

7

The useful life of Kapton® polyimide film is a function of both temperature and oxygen concentration. In accordance with UL-746B test procedures, the thermal life of Kapton® was determined at various temperatures. At time zero and 325°C (617°F), the tensile strength is 234 MPa (34,000 psi) and the elongation is 67%. The results are shown in **Figures 6–8**.

Figure 6.   Tensile Strength vs. Aging in Air at 325°C (617°F), Type HN Film, 25 μm (1 mil)
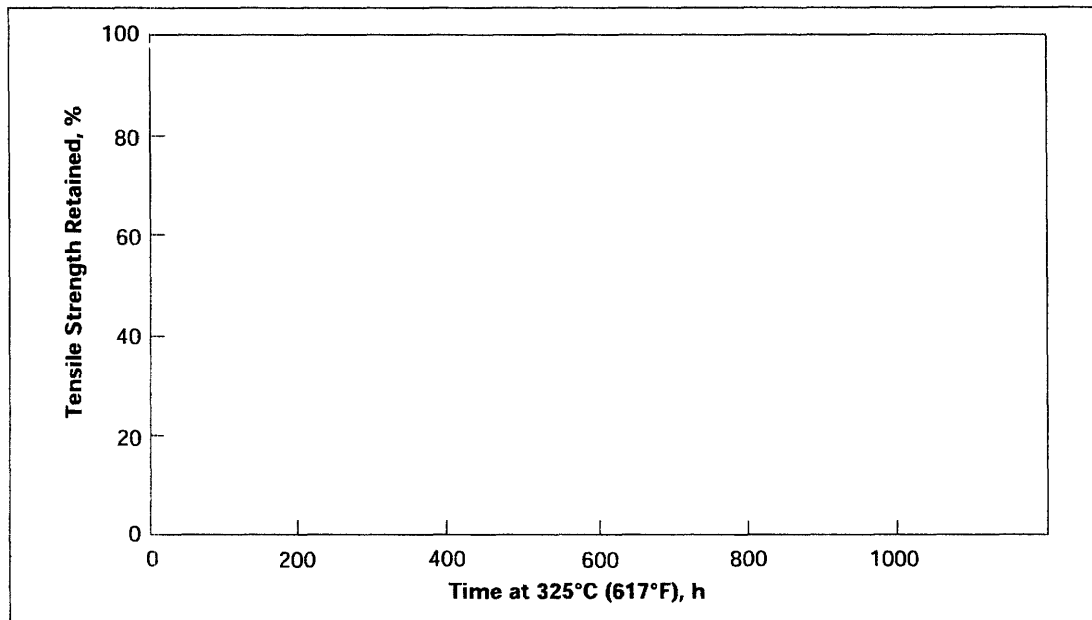

Figure 7.   Ultimate Elongation vs. Aging in Air at 325°C (617°F), Type HN Film, 25 μm (1 mil)
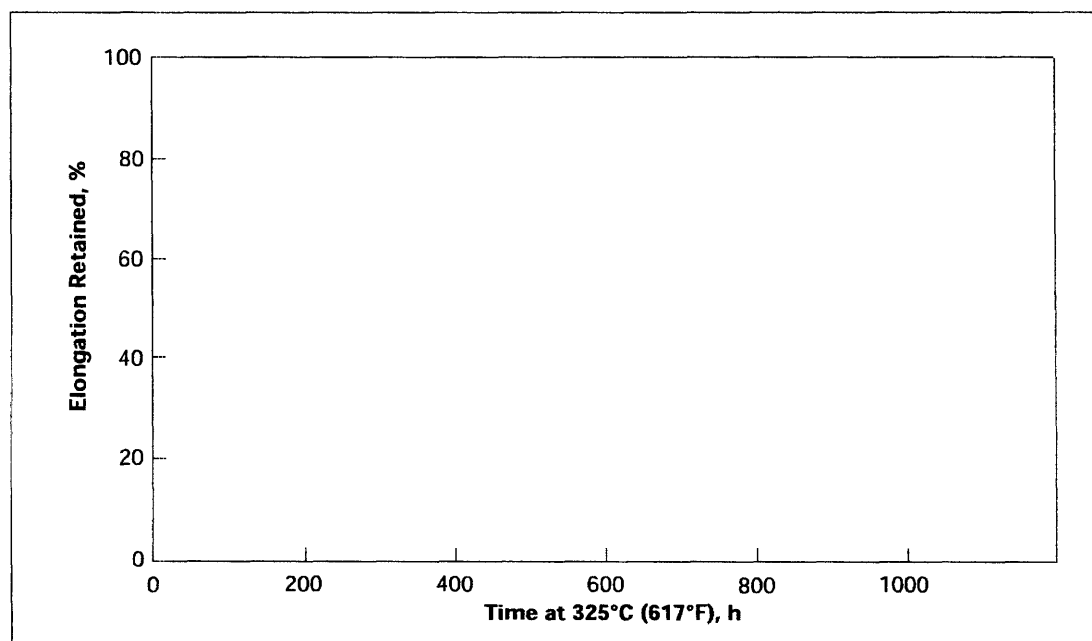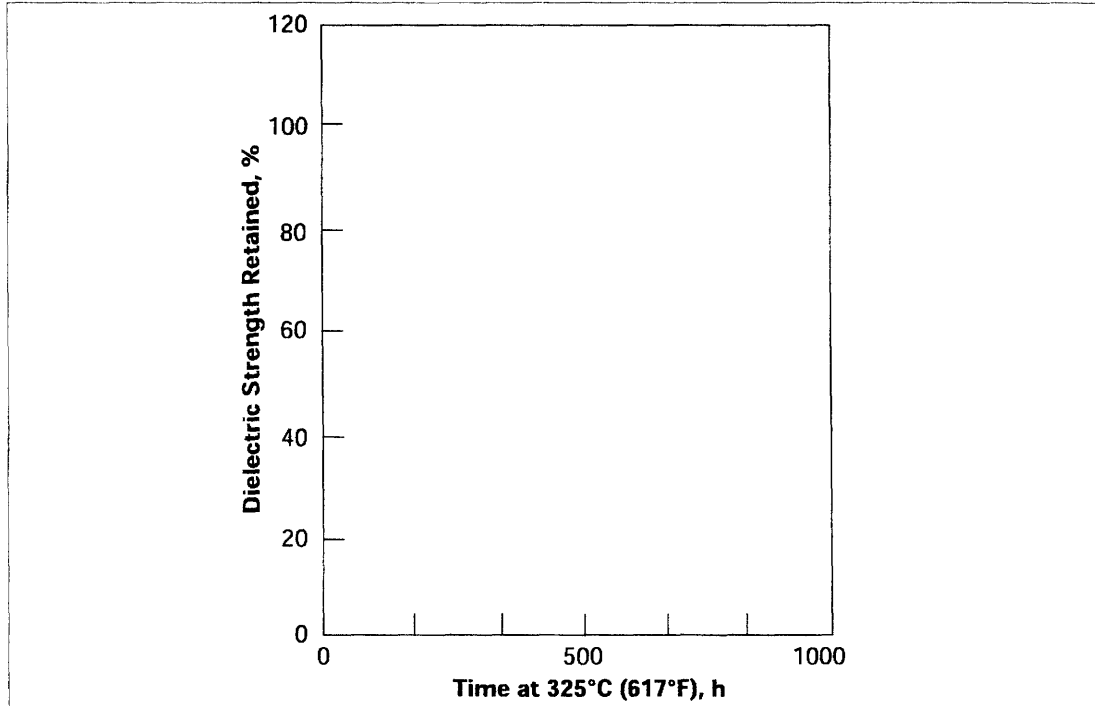

8

Figure 8. Retained Dielectric Strength at 325°C (617°F) for 25 μm (1 mil) Film, Test Method UL-746B

The life of Kapton® polyimide film at high temperature is significantly extended in a low-oxygen environment. Kapton® is subject to oxidative degradation. Hence, when it was tested in a helium environment, its useful life was at least an order of magnitude greater than in air. Using a DuPont 1090 thermal analyzer system, the weight loss characteristics of Kapton® in air and helium at elevated temperatures are shown in **Figures 9** and **10**.

Figure 9. Weight Loss, Type HN Film, 25 μm (1 mil)*
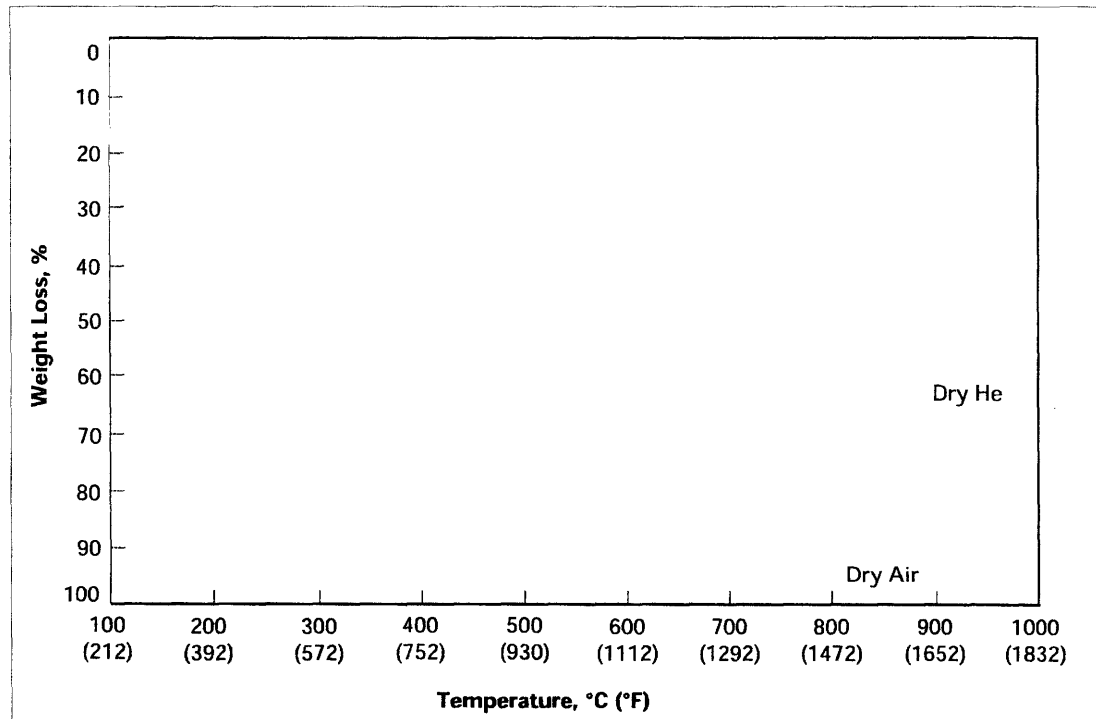
*Rate of temperature rise in °C (°F) was 3°C/min (5.4°F/min).

9

51